



Spatio-temporal variation in size-structured populations using fishery data: an application to shortfin mako (*Isurus oxyrinchus*) in the Pacific Ocean

Journal:	<i>Canadian Journal of Fisheries and Aquatic Sciences</i>
Manuscript ID	cjfas-2016-0327.R1
Manuscript Type:	Article
Date Submitted by the Author:	11-Nov-2016
Complete List of Authors:	Kai, Mikihiro; National Research Institute of Far Seas Fisheries, Fishery Research Agency, Thorson, James T.; Northwest Fisheries Science Center, National Marine Fisheries Service, NOAA Piner, Kevin; Southwest Fisheries Science Center, National Marine Fisheries Service, National Oceanic and Atmospheric Administration, Maunder, Mark; Inter-American Tropical Tuna Commission
Keyword:	spatio-temporal model, catch per unit effort, length data, shortfin mako, template model builder

SCHOLARONE™
Manuscripts

1 Spatio-temporal variation in size-structured populations using fishery data: an application to shortfin
2 mako (*Isurus oxyrinchus*) in the Pacific Ocean

3

4 Mikihiro Kai¹, James T. Thorson², Kevin R. Piner³, and Mark N. Maunder^{4,5}

5

6 ¹National Research Institute of Far Seas Fisheries (NRIFSF), Japan Fisheries Research and Education

7 Agency

8 5-7-1, Orido, Shimizu, Shizuoka 424-8633, Japan

9 ² Fisheries Resource Analysis and Monitoring Division, Northwest Fisheries Science Center, National

10 Marine Fisheries Service (NMFS), NOAA

11 2725 Montlake Boulevard E, Seattle, WA 98112, USA.

12 e-mail: james.thorson@noaa.gov

13 ³Southwest Fisheries Science Center, National Marine Fisheries Service (NMFS), NOAA

14 8901 La Jolla Shores Drive, La Jolla, CA 92037, USA.

15 e-mail: Kevin.Piner@noaa.gov

16 ⁴Inter-American Tropical Tuna comission

17 8604 La Jolla Shores Drive, La Jolla, CA 92037-1508, USA.

18 e-mail: mmaunder@iattc.org

19 ⁵Center for the Advancement of Population Assessment Methodology, Scripps Institution of

20 Oceanography, La Jolla, CA 92093, United States

21 *Correspondence to M Kai:

22 Tel(Fax): +81-543-36-6035

23 e-mail: kaim@affrc.go.jp

24

25 **Abstract**

26 We develop a length-disaggregated spatio-temporal delta-generalized linear mixed model
27 (GLMM) and apply the method to fishery-dependent catch rates of shortfin mako sharks in the North
28 Pacific. The spatio-temporal model may provide an improvement over conventional time-series and
29 spatially stratified models by yielding more precise and biologically interpretable estimates of abundance.
30 Including length data may provide additional information to better understand life history and habitat
31 partitioning for marine species. Nominal catch rates were standardized using a GLMM framework with
32 spatio-temporal and length composition data. The best fitting model showed that most hotspots for
33 “Immature” shortfin mako occurred in the coastal waters of Japan, while hotspots for “Subadult and adult”
34 occurred in the offshore or coastal waters of Japan. We also found that size specific catch rates provide an
35 indication that there has been a recent increasing trend in stock abundance since 2008.

36

37 **Keywords:** spatio-temporal model, catch per unit effort, length data, shortfin mako, template model
38 builder

39

40 **1. Introduction**

41 Reliable indices of population abundance are an important type of data for stock assessment
42 (Francis 2011). For stocks lacking designed fishery independent surveys, fishery catch-per-unit effort
43 (CPUE) data provide information on trends in stock abundance that is otherwise missing. Abundance
44 indices provide not only trends, but can be used to estimate population scale when combined with catch in

45 population dynamic models (Lee et al. 2014). Key to the use of these data is the assumption that the
46 change in the index is proportional to changes in population abundance (Wilberg et al. 2010). Much
47 attention has been devoted to estimation of CPUE from fishery dependent catches and effort (Maunder
48 and Punt 2004). Methods for standardizing CPUE data rely on introduction of auxiliary information to
49 separate changes due to changing population abundance from those due to changes due to fishing
50 practices and other factors. For widely dispersed stocks, the effects of spatial heterogeneity of both fish
51 and fisheries need to be considered with respect to the assumption of proportionality between estimates of
52 CPUE and population abundance. This becomes even more important when large areas of the stock
53 distribution receive little or no effort and assumptions about these areas becomes influential on estimates
54 of stock trend (Walters 2003; Carruthers et al. 2010; Carruthers et al. 2011).

55 Spatio-temporal modeling methods have been introduced to deal with spatial variation in
56 population distribution and density. Spatio-temporal methods can be used to estimate population
57 abundance indices using formal statistical tools such as likelihood functions and sampling designs (Bez
58 2002; Kristensen et al. 2014; Nishida and Chen 2004; Petitgas et al. 2014; Petitgas 1998; Roa-Ureta and
59 Niklitschek 2007; Thorson et al. 2015b, 2015c). Recent studies show that the approach may yield more
60 precise, biologically reasonable, and interpretable estimates of abundance than common methods such as
61 GLM (generalized linear model) and GLMM (generalized linear mixed model) (Shelton et al. 2014;
62 Thorson et al. 2015b) by reducing sample selection bias and filling in the spatial gaps common in
63 fishery-dependent data (Walter et al. 2014; Carruthers et al. 2011; Thorson et al. 2016).

64 Spatial and temporal changes in the size (or age) structure of the population is an important
65 aspect of the population abundance because marine fishes such as billfishes and oceanic pelagic sharks
66 show evidence of spatial size (or age/stage) segregation (Nakano and Nagasawa 1996; Piner et al. 2013).

67 Inclusion of auxiliary information about length into spatio-temporal methods allows prediction of the
68 annual trends of the standardized CPUE by length which may better accounts for changes in spatial
69 patterns of size structure of the stock. Kristensen et al. (2014) developed a spatio-temporal dynamics
70 model for Skagerrak cod (*Gadus morhua*) and Thorson et al. (2015a) developed a stage-structured model
71 for rex sole (*Glyptocephalus zachirus*) in the Gulf of Alaska using information from different types of
72 survey gear. These models incorporated size-structured information and described abundances of
73 different size classes and spatial bycatch risk. It would be therefore useful to illustrate the temporal
74 changes in the size specific CPUE using the fishery dependent data for pelagic sharks, which could be
75 used to distinguish juvenile and nursery habitats for these species, similar to recent length-structured
76 spatio-temporal analysis of survey trawls for shallow-water hake in the Benguela current (Jansen et al.
77 2016).

78 Shortfin mako (*Isurus oxyrinchus*) is a large and highly migratory shark species, and is widely
79 distributed in the Pacific Ocean between 50°N to 50°S (Compagno 2001). Shortfin mako is susceptible to
80 overexploitation due to slow growth rates, maturity at a late age, and low fecundity (Compagno 2001).
81 Female shortfin mako attain maturity at a much larger size and older age (256 cm PCL: pre-caudal length
82 / approximately 17 years old) than males (156 cm PCL / approximately 5 years old) (Semba et al. 2011).
83 In the western and central North Pacific, mainly 60-240 cm PCL (0-20 years old) individuals are caught
84 as bycatch by Japanese commercial pelagic longline fisheries targeting tuna and billfish (Kai et al. 2015).
85 Standardized CPUE of shortfin mako in the North Pacific were estimated using the onboard observer data
86 from 1995 to 2010, however, the historical trends of population abundance were poorly estimated due to
87 the misspecification of the model (See Table 1. Clarke et al. 2013). Therefore, improvement of the
88 estimates is needed to assess the status of shortfin mako stocks with greater accuracy and precision.

89 The objectives of this paper are to develop a length-disaggregated spatio-temporal delta-GLMM
90 using fishery-dependent catch-rate data and to apply the method to shortfin mako in the western and
91 central North Pacific. This method is used to predict not only the temporal (yearly) changes in the CPUE
92 but also the spatio-temporal distribution of CPUE for the different growth stages (size classes) of shortfin
93 mako. Improvements in both standardized CPUE and understanding of spatial patterns of shortfin mako
94 should result in better assessment and management of the stock.

95

96 **2. Materials and Methods**

97 **2.1. Data sources**

98 Catch and effort data of Japanese shallow-set longliners operating in the western and central
99 North Pacific from 2006 to 2014 were used to estimate the spatio-temporal variation in population density
100 for shortfin mako in the last nine years. We have a long time series of the catch and effort data from 1994
101 to 2014 but we used the data from 2006 to 2014 due to the limitation of the reliable length data. The
102 set-by-set data used in this study included information on species of sharks, catch number, amount of
103 effort (number of hooks), number of branch lines between floats (hooks between floats: HBF) as a proxy
104 for gear configuration, and location (longitude and latitude) of set, with a resolution of 2×2 degree
105 square. Only the shallow-set data were used in the analysis. The shallow-set data could be determined
106 because fishermen changed the depth of the gear to change the target species, and the number of HBF
107 varied depending on the depth (Nakano et al. 1997). We defined the shallow-set fishery by the use of a
108 small number of HBF (3 - 5). The hooks of the regular longline gear using these HBFs are estimated to
109 hang at the depth around 50 to 120 m (Suzuki et al. 1977).

110 The National Research Institute of Far Seas Fisheries in Japan commenced a project to collect the
111 length data of shortfin mako caught by Japanese coastal and offshore longline fishery in 2003. The
112 fishermen in the Kesenuma fishing port measure the precaudal length (PCL) of shortfin mako on the
113 boat. The Kesenuma fishing port is located in the northeast part of the Japanese mainland and it is well
114 known for its large landings of tuna, billfish and sharks (Ishimura and Bailey 2013). The longliner
115 recorded the size and other auxiliary information such as sex and exact location of the starting position of
116 each sets in addition to the information of the logbook data. We used the length data during 2006 and
117 2014 because many inaccurate records were included in the earlier periods during 2003 and 2005. The
118 size data of each individual caught by shallow set longliner was collated with the catch record of shortfin
119 mako in the logbook of the longline boat with a resolution of 2 x 2 degree square and year and quarter.
120 We then multiplied the catch rates from length-aggregated catch records by the proportion-at-size in the
121 longliner logbook data and analysed these length-disaggregated catch rates. When a given 2x2 square did
122 not have both longliner catch records and logbook data in a given quarter or year, we did not include that
123 location in that time period in the model. Available data include the average location and time of all sets
124 with a resolution of 2 x 2 degree square and year and quarter. The detailed information about the data
125 aggregation was summarized in Appendix A (Table A1).

126 The available data covered core areas of shortfin mako catch in the western and central North
127 Pacific (24 -44°N and 138°E -160°W) (Fig. 1) and four seasons. Four seasons (quarters 1 to 4) were
128 defined as follows: Q1 was spring from January to March; Q2 was summer from April to June; Q3 was
129 fall from July to September; and Q4 was winter from October to December. The fishery data provide
130 enough quantitative data to estimate the year-specific changes in the species distribution function and
131 relative trends of CPUE for growth stages of shortfin mako in the western and central North Pacific.

132 Three growth stages were defined as follows: “Juvenile” denotes the body size smaller than 90 cm PCL
133 (age-0), “Immature” denotes the body size between 90 cm and 160 cm PCL, and “Subadult and adult”
134 denotes the body size larger than 160 cm PCL.

135

136 **2.2. Spatio-temporal model with length composition data**

137 Size and CPUE data originate from two different sampling processes, such that length
138 measurement and catch per shot are not always directly matched. Then, the density estimate per station
139 (i.e. grid cell) is informed by the CPUE data and then decomposed by the estimated contribution of each
140 size class. The decomposition of the CPUE trend into individual size classes is the novel feature in this
141 study. Previous studies that incorporated auxiliary length information into spatial and temporal models
142 (Kristensen et al. 2014; Nielsen et al. 2014; Thorson et al. 2015a; Jansen et al. 2016) have focused on
143 research trawl survey data based on underlying randomly stratified sampling designs, whereas we attempt
144 to fit both length and CPUE to shallow-set longline fishery data. The fisheries-dependent data is collected
145 from a highly unbalanced sampling design due to systematic changes in the spatial effort allocation and
146 targeting behavior of the fleet (Carruthers et al. 2010, 2011; Thorson et al. 2016). A spatio-temporal
147 modeling approach can in some cases account for fishery targeting occurring at large spatial scales, and is
148 therefore appropriate to account for some common forms of bias that arise when analyzing in
149 fishery-dependent catch rates (Thorson et al. 2016).

150 We develop a model that accounts for both size-specific spatio-temporal variabilities in the
151 distribution and the relative trends of catch rate of shortfin mako in the last nine years in the western and
152 central North Pacific. We use a length-structured spatio-temporal model for this task, so that we can
153 explicitly decompose variance into additive components representing variation among years and size

154 classes (Krisensen et al. 2014). We then use the model to predict density at unsampled locations, times
155 and length classes, to provide a best-estimate of the distribution of species, relative trends of total
156 abundance, and length compositions. Spatio-temporal and length modelling of CPUE data assumes that
157 nearby locations and nearby size classes should have similar density estimates during each time interval.
158 The correlation between statistical stations (latitude and longitude) and length classes (length bins) in a
159 given interval is then used to estimate density in each year for all stations and length classes, including
160 stations and length bins that do not have data in a given period. We then visualize the predictions of
161 spatio-temporal variation in density and the temporal (yearly) changes in the total abundance for the
162 different growth stages (size classes).

163

164 **2.3. Model description**

165 The spatio-temporal model incorporating length data estimated the density $d(s, t, q, l)$ in each
166 station s (latitude and longitude with a resolution of 2×2 degree square), year t (where $t=1$ in signifies
167 2006 and $t=9$ signifies 2014), quarter q (signifying a three-month quarter, where $q=1$ in signifies
168 Q1(Jan-March) and $q=4$ in signifies Q4(Oct-Dec)) and body length l (bin #1: 50-80 cm; #2: 80.1-90cm;
169 #3: 90.1-100, ..., #12: 180.1-190 cm; #13: 190.1-340 cm., e.g., where the first bin is all individuals less
170 than or equal to 80cm, and the last bin is all individuals greater than 190 cm). After estimating parameters,
171 we then calculate juvenile density as the sum of density for 50-80 cm and 80.1-90 cm (i.e., the 1st and 2nd
172 length bins), immature as the sum of density for 90.1-100 cm to 150.1-160 cm (i.e., the 3rd to 9th length
173 bins), and subadult and adult as density for larger than 160.1 cm (i.e., the sum of the 10th to 13th length
174 bins).

175 We modeled variation in density among both years and quarters, to capture both annual trends in
 176 abundance and quarterly changes in catch rates. Each station, year, quarter and length-bin had the density:

$$177 \quad d(s, t, q, l) = \exp \left(d_0(t) + \gamma(s) + \tau(l) + \theta(s, t, l) + \delta(q) + \sum_{j=1}^{n_j} \beta_j x_j(s, t, q, l) \right) \quad (1)$$

178 where $d_0(t)$ represents intercept for year t , $\gamma(s)$ represents spatial variation (the average density in
 179 station s relative to the average station), $\tau(l)$ represents the non-parametric impact of length on expected
 180 catch rates (the average density in length l relative to the average length), $\theta(s, t, l)$ represents an
 181 interaction term and spatio-temporal and length variation (variation in density for station s , year t and
 182 length l after accounting for spatial, temporal and length variation), $\delta(q)$ is an offset that represents the
 183 impact of quarter (q) on average density, β_j is the effect of the j^{th} covariate on predicted density, and
 184 $x_j(s, t, q, l)$ is the value of the j^{th} covariate for a given location, year, quarter, and length-category. In the
 185 following, we use as covariate the length of the individual (i.e., $n_j = 1$ and $x(s, t, q, l) = l$), which
 186 generates a log-linear increase or decrease in expected density with length, but future research could
 187 incorporate additional habitat variables. The marginal (common to all spatial stations and times) length
 188 variation, $\tau(l)$, is modeled using a first-order autoregressive process (AR1) to explain the correlations
 189 among length bins.:

$$190 \quad \boldsymbol{\tau} \sim \text{MVN}(0, \sigma_{\boldsymbol{\tau}}^2 \mathbf{R}_{\boldsymbol{\tau}}) \quad (2)$$

191 where MVN is a multivariate normal distribution with mean 0 correlation matrix $\mathbf{R}_{\boldsymbol{\tau}}$, and pointwise
 192 variance $\sigma_{\boldsymbol{\tau}}^2$:

$$193 \quad \mathbf{R}_{\boldsymbol{\tau}}(l, l') = \rho_{\boldsymbol{\tau}}^{|l-l'|} \quad (3)$$

194 where $\rho_{\boldsymbol{\tau}}$ is a parameter governing autocorrelation, while $|l-l'|$ is the difference in length among samples
 195 in length-bin l and l' . $\rho_{\boldsymbol{\tau}}$ is the magnitude of autoregression (where $\rho_{\boldsymbol{\tau}} = 0$ implies that all lengths are
 196 statistically independent, while $\rho_{\boldsymbol{\tau}} = 1$ implies that total density approaches a random-walk process

197 among lengths). The model (Eq. (1)) includes both a parametric effect of length (by including a log-linear
 198 impact of length on expected catch using parameter β_j) and a non-parametric effect of length (by
 199 including a first-order autoregressive component using $\tau(l)$). We therefore interpret this as a
 200 “semi-parametric” model with respect to the impact of length on catch rates (e.g., Kristensen 2014;
 201 Thorson and Taylor 2014).

202 Spatial variation $\gamma(s)$ is modeled as a Gaussian random field (GRF), which reduces to a
 203 multivariate normal distribution when evaluated at a finite set of stations (Thorson et al. 2015c):

$$204 \quad \boldsymbol{\gamma} \sim \text{MVN}(\mathbf{0}, \boldsymbol{\Sigma}_{\text{spatial}}) \quad (4)$$

205 where $\boldsymbol{\Sigma}_{\text{spatial}}$ is spatial covariance for the random field and approximated using a Matérn correlation
 206 function with smoothness $\nu = 1$:

$$207 \quad \boldsymbol{\Sigma}_{\text{spatial}}(s, s') = \frac{\sigma_\gamma^2}{\Gamma(\lambda)2^{\lambda-1}} \cdot (\kappa|\mathbf{H}(s - s')|)^\nu K_\nu(\kappa|\mathbf{H}(s - s')|) \quad (5)$$

208 where $|s-s'|$ is the Euclidian distance between two generic locations s and s' , σ_γ is the marginal variances
 209 of the spatial random field, Γ is the gamma function, and K_ν is the modified Bessel function of second
 210 kind (Lindgren et al. 2011). This covariance function calculates the correlation between $\boldsymbol{\gamma}$ at stations s
 211 and s' given their distance $|s-s'|$ after linear transformation \mathbf{H} which accounts for geometric anisotropy
 212 (see supplementary in Thorson et al. 2015a). If the spatial covariance structure is equivalent in all
 213 directions, it can be described as a function of distance only and is said to be isotropic (i.e. \mathbf{H} is a
 214 two-dimensional identity matrix). If the spatial covariance structure varies in different directions, then it is
 215 a function of the distance and direction and is said to be anisotropic (where the directions of slow and fast
 216 decorrelation are given by \mathbf{H}). Isotropic processes form an inadequate basis in modelling many spatially
 217 distributed data, while \mathbf{H} is essentially a linear transformation of coordinates as is common for
 218 estimating stationary anisotropy (Budrikaite and Ducinskas 2005). $\kappa > 0$ is a scaling parameter related to

219 the range that means the distance at which the spatial correlation becomes almost null. We use a
 220 stochastic partial differential equation (SPDE) approximation to this function, and can calculate the
 221 geostatistical range ($\frac{\sqrt{8\nu}}{\kappa}$) as the distance at which correlation is close to 10 %, for each smoothness
 222 parameter $\nu > 1/2$ (Lindgren et al. 2011). We used the Matérn correlation function because previous
 223 research demonstrated how the probability of GRFs could be calculated efficiently given this assumption
 224 (Diggle and Ribeiro 2007; Lindgren et al. 2011; Roa-Ureta and Niklitschek 2007). GRF is a convenient
 225 statistical approach for implementing a 2-dimensional smoother for a response variable (in this case,
 226 catch) over spatial dimensions (Thorson et al. 2015b). The spatio-temporal and length variation, $\theta(s, t, l)$,
 227 is modeled by combining the GRF for spatial variation with first-order autoregressive process (AR1) for
 228 temporal and length variation:

$$229 \quad \text{vec}(\boldsymbol{\theta}_t) \sim MVN(\mathbf{0}, \boldsymbol{\Sigma}_{\text{spatial}} \otimes \mathbf{R}_\theta) \quad (6)$$

230 where $\text{vec}(\boldsymbol{\theta}_t)$ is the vectorized value of $\theta(s, t, l)$ for all stations and length-bins in year t , \otimes is the
 231 Kronecker product where if \mathbf{A} is an $m \times n$ matrix and \mathbf{B} is a $p \times q$ matrix, then the Kronecker product
 232 $\mathbf{A} \otimes \mathbf{B}$ is the $mp \times nq$ block matrix:

$$233 \quad \mathbf{A} \otimes \mathbf{B} = \begin{bmatrix} \mathbf{a}_{11}\mathbf{B} & \cdots & \mathbf{a}_{1n}\mathbf{B} \\ \vdots & \ddots & \vdots \\ \mathbf{a}_{m1}\mathbf{B} & \cdots & \mathbf{a}_{mn}\mathbf{B} \end{bmatrix}, \quad (7)$$

234 \mathbf{R}_θ is the correlation in $\boldsymbol{\theta}_t$ among length-bins

$$235 \quad \mathbf{R}_\theta(l, l') = \rho_\theta^{|l-l'|} \quad (8)$$

236 where ρ_θ is a parameter governing autocorrelation among length bins for the spatio-temporal variance
 237 component. In the following, $\delta(q)$ represents a increase or decrease in expected catch rates for each
 238 quarter relative to the 1st quarter ($\delta(1) = 0$ to ensure identifiability). We included both the covariate
 239 length as well as the AR1 for length variation, and we interpret this as a semi-parametric specification of
 240 the effect of length on expected catch rates. We estimated a separate standard deviation for spatial (σ_γ)

241 and spatio-temporal and length (σ_θ) components, but estimated the same decorrelation distance (κ) for
 242 the processes, using the implicit assumption that dynamics were defined by a “characteristic scale” that
 243 defined decorrelation distance for each of them. Following the parameterization from Lindgren et al.
 244 (2011), we estimated a magnitude parameter η for each spatial (η_γ) and spatio-temporal and length (η_θ)
 245 process and the corresponding standard deviation was then calculated as:

$$246 \quad \sigma_\gamma = 1/\sqrt{4\pi\eta_\gamma^2} \quad (9)$$

247 where the other standard deviation (i.e., σ_θ) was calculated similarly (from η_θ). Aside from this, we also
 248 estimated a magnitude parameter η for length (η_τ) process.

249 Expected catch λ_i is a function of density and fishing effort f_i (number of hooks), $\lambda_i =$
 250 $d(s_i, t_i, q_i, l_i)f_i$, and is compared with the observed catch (in numbers) c_i for the i -th observation, in
 251 station s_i , year t_i , quarter q_i and length l_i . Count data of the sharks typically included many observations
 252 with zero catch and a few observations with large values when the sharks were aggregated (Bigelow et al.
 253 1999; Ward and Myers 2005). Population trends of by-catch species such as sharks are commonly
 254 estimated using the delta lognormal model to account for the occurrence of excess zeros (Lo et al. 1992;
 255 Zuur et al. 2009) and the negative binomial model or gamma model to account for overdispersion
 256 (Brodziak and Walsh 2013). The delta lognormal model is a combination of the probability of non-zero
 257 catches (“encounter”) assuming a logistic model and the probability of positive catch rates (“catch rates
 258 for each encounter”) assuming a log-normal model.

259 Because the compiled spatio-temporal data of shortfin mako showed evidence of excess zeros
 260 (51.3%) and the dispersion ratio (variance/mean = 34.9), we assume that available catch data c arises from
 261 the following delta (a.k.a. two stages) model, where the probability that a given sample is non-zero:

$$262 \quad \Pr(C > 0) \equiv p = \left(\frac{1}{1 + \exp(-z_0)} \right) \times (1 - \exp(-z_1\lambda)) \quad (10)$$

263 where z_0 governs the encounter probability given very high local densities (i.e., $p \rightarrow \frac{1}{1+\exp(-z_0)}$ as
 264 $\lambda \rightarrow \infty$), and z_1 governs how the probability of encounter increases with local expected catch λ .

265 Catches then follow a lognormal distribution or a gamma distribution:

$$266 \quad \Pr(C = c | c > 0) = \text{Lognormal} \left(C; \log\left(\frac{\lambda}{p}\right), \sigma^2 \right) \quad (11)$$

$$267 \quad \Pr(C = c | c > 0) = \text{Gamma} \left(C; \frac{1}{CV^2}, \frac{\lambda CV^2}{p} \right) \quad (12)$$

268 where Lognormal ($x; m, \sigma^2$) is the lognormal probability density function evaluated at x , given log-mean
 269 m and log-standard deviation σ , σ is the time-varying (i.e. yearly changes in) log-standard deviation for
 270 catch rates given an encounter, Gamma ($x; \alpha, \beta$) is the probability density function of a gamma
 271 distribution with shape α and scale β , evaluated at x , CV is the coefficient of variations for catch rates
 272 given an encounter, and these equations are defined such that $median(C) = \lambda$.

273 Parameters representing temporal (year) variance (d_0), spatial covariance (κ and η_γ), length
 274 variance (ρ_τ and η_τ), spatial-temporal and length covariance (κ , ρ_θ and η_θ), covariates of respective
 275 length (β) and quarter (δ), and residual variation (σ) were estimated as fixed effects while integrating
 276 across random effects representing spatial (station), length, and spatio-temporal and length variations (see
 277 Appendix Table A2). This integral was approximated using the Laplace approximation, and the fixed
 278 effects were estimated using gradient information as provided by Template Model Builder (TMB), which
 279 is an R package (R Core Team 2013) for fitting statistical latent variable models to data. It was inspired by
 280 ADMB (Fournier et al. 2012). The details of TMB are described by Kristensen et al. (2016). Further
 281 details regarding GRF estimation can be found in Thorson et al. (2015b, 2015c).

282 After estimating the fixed effects by maximizing the marginal likelihood of the data, the
 283 distribution of catch rates of shortfin mako were predicted from the random effects using Empirical Bayes
 284 (i.e., by fixing them to the value that maximizes the joint likelihood with respect to random effects, while

285 fixed effects are set to their maximum likelihood estimates; Appendix B). We used a recent
286 bias-correction algorithm to account for retransformation bias when predicting and visualizing total
287 abundance and size composition (Thorson and Kristensen 2016). Model convergence was confirmed by
288 ensuring that the hessian matrix was positive definite and that the absolute-value of the final gradient of
289 parameters was less than 0.1.

290

291 **2.4. Model selection and diagnostics**

292 We selected the most parsimonious model using Akaike Information Criterion (AIC; Akaike
293 1974) and percent deviation (Maunder and Punt 2004). AIC identifies which model greater support had
294 given available data: this model-selection is appropriate given that TMB implements maximum marginal
295 likelihood estimation (Hoeting et al. 2006, Thorson et al. 2015c). Latter methodology examined a
296 common ad hoc response that is to require each addition of model complexity to explain more than some
297 agreed minimum (0.5 % was arbitrarily given) of additional percent deviation (%) explained (Maunder
298 and Punt, 2004). First, we chose the best model with regards to the error distribution of positive catch part
299 in the zero-inflated model and the necessity of the anisotropy from the following four models:

300 Model-A: delta-lognormal distribution model without anisotropy,

301 Model-B: delta-lognormal distribution model with anisotropy,

302 Model-C: delta-gamma distribution model without anisotropy,

303 Model-D: delta-gamma distribution model with anisotropy,

304 where the full model in Eq. (1) was used for these models. Second, we chose the best model with regards
305 to the combinations of the explanatory variables for the selected model in the first model selection. We
306 also compared the yearly changes in predicted catch rates among multiple models for first and second

307 model selection. Coefficient of variations (CV) and confidence intervals of annual changes in the CPUE
308 were calculated for the best-fitting model using the information matrix and delta-method (Fournier et al.
309 2012). We also examined the standard regression diagnostic statistics for the best-fitting model to identify
310 model misspecification and heteroscedascity (Maunder and Punt 2004).

311

312 **3. Results**

313 The delta-lognormal distribution model with anisotropy and most complex model including
314 temporal (quarter), spatial (station), length (precaudal length) and spatio-temporal and length variances as
315 random effects was identified as the most parsimonious model by AIC (Table 1). Overall, the trend in
316 predicted CPUE was almost similar among four models, however, the difference of the error distribution
317 had a large impact on the trends in predicted CPUE in spite of the random field (Fig. 2a). The predicted
318 CPUE was slightly changed if we added sequentially random effect components to the null model (Fig.
319 2b). These results and the marginal standard deviation (SD) in Table 1B indicated that the interaction
320 terms and station had more impact on the changes in the trends than single length effect. Percent deviation
321 also supported the result of the model selection by AIC (Table 1). We also examined the goodness-of-fits
322 for the best fitting model using residual diagnostics plots (Appendix C). We then used the best fitting
323 model to predict both the temporal (yearly) changes in the CPUE and also the spatio-temporal distribution
324 of CPUE for the different growth stages of shortfin mako.

325 Average overall spatial distribution of the predicted CPUE showed that most of the hotspots for
326 shortfin mako were in the coastal (32–42 °N and 136–146 °E) and offshore (34–44 °N and 150–170 °E)
327 waters off Japan (Fig. 3a). The predicted CPUE in offshore water tended to be lower than those in the
328 coastal waters with the highest CPUE was found between 36–38 °N and 142–144 °E. The results were

329 similar to the spatial distribution of the nominal CPUE except that the CPUE is generally higher at the
330 northern boundary (Fig. 3b).

331 Predicted annual CPUE exhibited a slight decline to the lowest level in 2008, and then sharply
332 increased until 2009 and increased again in 2014 (Fig. 4). Uncertainty in CPUE estimates is larger in the
333 most recent years (2012-2014) than in the early years (2006-2008).

334 Predicted CPUE by pre-caudal length intervals (cm) was dome shaped with the highest CPUE
335 peaking at a length bin from 140 to 150 cm PCL (Fig. 5). This was a sharp contrast from the nominal
336 peak in CPUE which occurred at length bin from 110 to 120 cm PCL. The overall mean length of
337 predicted CPUE (146 cm PCL) was shifted to larger sizes compared to that of nominal CPUE (138 cm
338 PCL) because the nominal CPUE by size class represented the pooled length weighted by the data
339 (nominal catch divided by effort) and predicted CPUE by size class is weighted by area (predicted catch
340 based on the spatial effect divided by effort). Uncertainty in CPUE estimates is larger in the middle ranges
341 of the length classes (length from 110-170 cm PCL) than both sides (smaller than 100 cm PCL and larger
342 than 170 cm PCL).

343 The average spatial distribution of the predicted CPUE for the three growth stages (Fig.6) shows
344 that most of the hotspots for “Juvenile” shortfin mako smaller than 90 cm PCL were in the offshore
345 waters off Japan (Fig.6a), while most of the hotspots for “Immature” shortfin mako between 90 and 160
346 cm PCL were in the coastal waters off Japan (Fig.6b). Most of the hotspots for “Subadult and adult”
347 shortfin mako larger than 160 cm PCL (Fig. 6c) were in the offshore waters off Japan with some higher
348 CPUE located in coastal waters (34–36 °N and 138–142 °E). The predicted CPUE hotspots were similar
349 to those of nominal CPUE observations except that the nominal CPUE for juveniles was patchy (Fig.
350 6d-f).

351 Yearly changes in the predicted CPUE for different growth stages are shown in Fig.7 and Table
352 A3. The values in Table A3 was calculated using the equations in Appendix D. Predicted CPUE of
353 “Juvenile” shortfin mako had a decreasing trend except in 2009 and 2014 and high CPUE were observed
354 in 2006, 2009 and 2014 (Fig. 7a). The sharp increase in CPUE for juveniles from 2013 to 2014 was
355 unlikely to occur for a low fecundity species like shortfin mako. Predicted CPUE of “Immature” shortfin
356 mako illustrated a slight decline to the lowest level in 2008, and then gradually increased and approached
357 to approximately 1.5 in 2014 (Fig. 7b). The trends in the CPUE time series is strongly similar to those for
358 all size classes in Fig. 4 because Japanese shallow set longline fishery dominantly catch the immature size
359 classes between 90-160cm in PCL (see Fig. 5). The CVs of the predicted CPUE for “Immature” shortfin
360 mako were smaller than those for “Juvenile” and “Subadult and adult” shortfin mako (Table A3).
361 Predicted CPUE of “Subadult and adult” shortfin mako exhibited an increasing trend with larger CVs in
362 accordance with the length of the elapsed time (Table A3). The fishing effort (number of hooks) showed a
363 gradual decreasing trends since 2007, declining to approximately 0.5 million hooks in 2011 due to the
364 Great East Japan Earthquake. Fishing effort increased in 2012 and maintained at approximately 0.75
365 million hooks until 2014.

366 The spatial distributions of the predicted CPUE for different growth stages showed that the
367 locations of hotspots were not fixed through time (Fig. 8). “Juvenile” shortfin mako hotspots varied
368 primarily latitudinally with one instance of a coastal hotspot. For the others (i.e. “Immature”, “Subadult
369 and adult”, “All stages”), annual variability in hotspots of CPUE were high and the numbers of hotspots
370 were increased in more recent years than early years especially for “Subadult and adult” stage. During
371 2014 there was a particularly large hot spot for juveniles at the northern border, which probably caused
372 the dramatic increase in the CPUE index for juveniles in that year.

373 Predicted CPUE by pre-caudal length (cm) showed similar dome shapes across years (Fig. 9).
374 The years 2010 and 2013 were the most strongly peaked (at length bins from 140 to 150 cm PCL) with
375 the other years estimated to have broader peaked CPUE (130-160 cm PCL).

376

377 **4. Discussion**

378 We developed a length-disaggregated spatio-temporal delta-generalized linear mixed model and
379 applied the method to shortfin mako sharks in the North Pacific. Inclusion of auxiliary length data into the
380 spatio-temporal model provided a tool to better understand life history and habitat partitioning for marine
381 species such as shortfin mako shark.

382 Oceanic pelagic sharks such as a shortfin mako typically have relatively little reliable data
383 because of the low economic values of these sharks compared with the more valuable species such as
384 tuna and billfish (Bonfil 1994; Walker 1988). Because stocks of pelagic sharks are often data poor (e.g.,
385 shortfin mako, which only has reliable length data starting in 2006), fishery indicators such as CPUE
386 trends often provide the only information on stock status (ISC 2015). However, spatial shifts in fishing
387 operations and the large spatial boundaries of stocks has made standardization of fishery catch rates
388 problematic.

389 The spatio-temporal model used in this study predicted both density and length composition in
390 areas where there is no data or inadequate data by explicitly considering the correlation of the data
391 regarding the body length in addition to the space and time (Shelton et al. 2014; Thorson et al. 2015b).
392 Thorson et al. (2015b) raised a concern about the spatio-temporal model which may result in biased
393 estimates when fishing effort is correlated with population abundance (Diggle et al. 2010). However,
394 Japanese longline fishery does not target shortfin mako, so that this may not be a problem. It is true that

395 the spatio-temporal method will be subject to bias and increased variance if the hotspots of the shortfin
396 mako overlaps with those of other target species, but this should also be true with more classical
397 standardization methods.

398 In this study, we used a time varying standard deviation for the statistical model. The fitting to
399 the data could be better given a separate log-standard deviation for catch rates for each year because the
400 observation errors fluctuate with changes in the operational patterns of the fishery for each year, although
401 the number of the parameter is increased. In addition, it was shown that the inclusion of a stochastically
402 time-varying common variance component can lead to substantial improvements in the fit of the time
403 series (Bos and koopman 2010).

404 Generalized linear mixed model commonly bases the AIC on the marginal model with the
405 random effects integrated out which may lead model selection to favor including more covariates than is
406 optimal (Greven and Kneib 2010). Hoeting et al. (2006) demonstrated that the corrected AIC for a
407 spatio-temporal model was superior to the standard approach of ignoring spatial correlation in the
408 selection of explanatory variables. However, we used a standard AIC because the corrected AIC is similar
409 to the standard AIC for large sample size.

410 In this modeling, we did not explicitly account for the differences in distribution or density
411 between males and females because many records of length were associated with individuals for which
412 the sex was not measured. Oceanic pelagic sharks such as a shortfin mako show evidence of remarkable
413 sexual segregation in the estimated distribution (Mucientes et al. 2009) and sexual dimorphism occurs
414 (Bishop et al. 2006; Semba et al. 2009). Separately modelling spatio-temporal density for males and
415 females would allow future analyses to identify differences in spatial distribution (and potentially different
416 exploitation rates) for males and females as well as annual trends of the standardized catch rate by sex,

417 and we recommend this line of future research. The spatio-temporal maps might provide the geographical
418 segregation of species by sex from year to year and might be useful to identify the essential habitat such as
419 pupping grounds and mating grounds. Ohshimo et al. (2016) reported that there was no strong evidence
420 for sexual differences in the distribution patterns or environmental preferences for juvenile shortfin mako.
421 However, their survey periods and areas are limited, so it is valuable to repeat those studies using more
422 complete data in future work. Future spatio-temporal models could account for missing data about
423 individual sex by treating sex as a random effect (where observed catch rates follow a mixture distribution
424 with two components). However, this requires prior information regarding the proportion by sex for each
425 length category, and would therefore require further model development.

426 The analysis we present is generally applicable and should be considered as a standard tool in
427 fisheries stock assessment. CPUE data is typically standardized for factors such as area, season, and gear
428 characteristics to develop indices of relative abundance, but the most common procedures (e.g. GLMs)
429 give equal weight to each data point (Maunder and Punt 2004). However, since the index is supposed to
430 represent the whole stock, the data may not be evenly spread over all areas biasing the index and some
431 form of area weighting should be used. The spatio-temporal approach automatically provides area
432 weighting in addition to augmenting areas with no or little data (Thorson et al. 2015b). However, our
433 approach takes this one step further to include length structure in the analysis. Despite CPUE data being
434 standardized to produce an index of abundance, the accompanying composition data that is used to
435 estimate the selectivity representing the index (i.e. the age or size of fish represented by the index) is not
436 standardized or area weighted. Use of our approach would harmonize the use of CPUE and composition
437 data for creating indices of abundance for use in contemporary stock assessment models.

438 Hiraoka et al. (2016) reported that annual target shifts by Japanese shallow-set longliner
439 occurred seasonally and geographically; the greatest change in target species, from swordfish to blue
440 shark, occurred in spring (April–June). They used 10th percentile of the swordfish CPUE values to
441 incorporate this variable target behavior into the abundance index. We applied the same target indicator
442 (rank of swordfish CPUE) to reduce the influences of the target behavior on the CPUE prediction of
443 shortfin mako (Appendix E). The results indicated that the target changes between two target species had
444 a small impact on the annual trends in the CPUE of shortfin mako (Fig. A3). Since shortfin mako shark is
445 bycatch species unlike the swordfish and blue shark, the target shifts may not largely influence on the
446 trends in the CPUE.

447 We used state-of-the-art methods to standardize the catch and effort data, including extending
448 the geostastical method to include length data. Three conclusions were derived from the application study:
449 (1) most of the hotspots for “Immature” shortfin mako between 90 and 160 cm PCL occurred in the
450 coastal waters of Japan, while most of the hotspots for “Subadult and adult” larger than 160 cm PCL
451 occurred predominately in the offshore waters of Japan; (2) the predicted CPUE for the different growth
452 stages provided an indication that the recent stock trends of shortfin mako in the western and central
453 North Pacific was better than that in mid-2000s; (3) part of the juvenile population is probably outside the
454 range of the fishery during some years and therefore the CPUE based index of abundance for juveniles is
455 unreliable. Further research and testing of this promising approach is recommended towards making it a
456 widely applicable standard tool for fisheries assessments.

457

458 **Acknowledgements**

459 We sincerely wish to thank two anonymous reviewers, all members of the ISC shark Working
460 Group that made invaluable comments and suggestions. We also appreciate Ko Shiozaki who supported
461 to draw the clear map. We also thank Kasper Kristensen and the many contributors to the Template
462 Model Builder software. We sincerely appreciate the crews of the coastal and offshore longline fleet from
463 Kesenuma fishing port, Japan, for their full support in collecting samples from a wide range of the North
464 Pacific. Finally, we are extremely grateful for the great contributions of K. Ishida, T. Oyama, M. Onodera,
465 and S. Onodera who collected and measured the biological samples. This work was supported in part by a
466 grant-in-aid from the Japan Fisheries Agency.

467

468 **References**

- 469 Akaike, H. 1973. Information theory as an extension of the maximum likelihood principle. *In*: 2nd
470 International Symposium on Information Theory. Edited by Petrov, B.N., and Csaki, F. Akademiai
471 Kiado, Budapest. pp. 267–281.
- 472 Bez, N. 2002. Global fish abundance estimation from regular sampling: the geostatistical transitive method.
473 *Can. J. Fish. Aquat. Sci.* **59** (12): 1921–1931. doi:10.1139/f02-155.
- 474 Bigelow, K.A., Boggs, C.H., and He, X. 1999. Environmental effects on swordfish and blue shark catch
475 rates in the US North Pacific longline fishery. *Fish. Oceanogr.* **8** (3): 178–198.
- 476 Bishop, S.D.H., Francis, M.P., Duffy, C., and Montgomery, J.C. 2006. Age, growth, maturity, longevity and
477 natural mortality of the shortfin mako shark (*Isurus oxyrinchus*) in New Zealand waters. *Mar.*
478 *Freshwater Res.* **57** (2): 143–154. doi:10.1071/MF05077.
- 479 Bonfil, R. 1994. Overview of world elasmobranch fisheries. FAO Fish. Tech. Pap. 341.
- 480 Bos, C.S., and Koopman, S.J. 2010. Models with time-varying mean and variance: A robust analysis of
481 U.S. industrial production. Tinbergen Institute Discussion Paper, TI2010-017/4.

- 482 Brodziak, J., and Walsh, W.A. 2013. Model selection and multimodal inference for standardizing catch
483 rates of bycatch species: a case study of oceanic whitetip shark in the Hawaii-based longline fishery.
484 Can. J. Fish. Aquat. Sci. **70** (12): 1723–1740. doi: 10.1139/cjfas-2013-0111.
- 485 Budrikaite, A. and Ducinkas, K. 2005. Modeling of geometric anisotropic spatial variation. Proceeding
486 of the 10th International Conference MMA2005&CMAM2, Trakai.
- 487 Clarke, S.C., Harley, S.J., Hoyle, S.D., and Rice, J.S. 2013. Population trends in Pacific oceanic sharks
488 and the utility of regulations on shark finning. Conserv. Biol. **27** (1): 197–209. doi:
489 10.1111/j.1523-1739.2012.01943.x.
- 490 Compagno, L.J.V. 2001. Sharks of the World. An annotated and illustrated catalogue of shark species
491 known to date. Vol. 2. Bullhead, mackerel and carpet sharks (*Hetero dontiformes*, *Lamniforms* and
492 *Orectolobiformes*). FAO Spes. Cat. Fish. Purp. 1 (2), Rome, FAO.
- 493 Carruthers, T.R., McAllister, M.K. and Ahrens, R.N.M. 2010. Simulating spatial dynamics to evaluate
494 methods of deriving abundance indices for tropical tunas. Can. J. Fish. Aquat. Sci. **67**: 1409–1427.
- 495 Carruthers, T.R., Ahrens, R.N.M., Mcallister, M.K. and Walters, C.J. 2011. Integrating imputation and
496 standardization of catch rate data in the calculation of relative abundance indices. Fish. Res. **109**: 157–
497 167.
- 498 Diggle, P., and Ribeiro, P. 2007. Model-Based Geostatistics. Springer, New York.
- 499 Diggle, P.J., Menezes, R., and Su, T. 2010. Geostatistical inference under preferential sampling. J. R. Stat.
500 Soc. Ser. C Appl. Stat. **59** (2): 191–232. doi:10.1111/j.1467-9876.2009.00701.x.
- 501 Fournier, D.A., Skaug, H.J., Ancheta, J., Ianelli, J., Magnusson, A., Maunder, M.N., Nielsen, A., and Sibert, J.
502 2012. AD Model Builder: using automatic differentiation for statistical inference of highly parameterized
503 complex nonlinear models. Optim. Methods Softw. **27** (2): 233–249. doi:10.1080/10556788.2011.597854.

- 504 Francis, R.I.C.C. 2011. Data weighting in statistical fisheries stock assessment models. *Can. J. Fish. Aquat.*
505 *Sci.* **68** (6): 1124–1138. doi:10.1139/f2011-025.
- 506 Greven, S., and Kneib, T. 2010. On the behaviour of marginal and conditional AIC in linear mixed models.
507 *Biometrics.* **97** (4): 773–789. doi:10.1093/biomet/asq042.
- 508 Hiraoka, Y., Kanaiwa, M., Ohshimo, S., Takahashi, N., Kai, M., and Yokawa, K. 2016. Trend in the
509 relative abundance of the blue shark *Prionace glauca* based on the activities of Japanese distant water
510 and offshore longliners in the North Pacific. *Fish. Sci.* **82**: 687-699.
- 511 Hoeting, J.A., Davis, R.A., Merton, A.A., and Thompson, A.E. 2006. Model selection for geostatistical
512 models. *Ecol. Appl.* **16** (1): 87–98. doi:10.1890/04-0576.
- 513 ISC, 2015. Indicator-based analysis of the status of shortfin mako shark in the north Pacific Ocean. Report
514 of the Shark Working Group. Kona, Hawaii. USA. Available from [http://](http://http://isc.fra.go.jp/pdf/ISC15/Annex%2012_SMA%20stock%20assessment%20report%20(2015)%2030Jul15_changes%20accepted.pdf)
515 [http://isc.fra.go.jp/pdf/ISC15/Annex%2012_SMA%20stock%20assessment%20report%20\(2015\)%2030Jul15_changes%20accepted.pdf](http://isc.fra.go.jp/pdf/ISC15/Annex%2012_SMA%20stock%20assessment%20report%20(2015)%2030Jul15_changes%20accepted.pdf) [accessed 18 January 2017]
- 516
- 517 Ishimura, G., and Bailey, M. 2013. The market value of freshness: observations from the swordfish and
518 blue shark longline fishery. *Fish. Sci.* **79** (3): 547–533. doi: 10.1007/s12562-013-0609-6.
- 519 Jansen, T., Kristensen, K., Kainge, P., Durholtz, D., Strømme, T., Thygesen, U.H., Wilhelm, M.R.,
520 Kathena, J., Fairweather, T.P., Paulus, S., Degel, H., Lipinski, M.R., and Beyer, J.E. 2016. Migration,
521 distribution and population (stock) structure of shallow-water hake (*Merluccius capensis*) in the
522 Benguela Current Large Marine Ecosystem inferred using a geostatistical population model. *Fish. Res.*
523 **179**: 156–167. doi:10.1016/j.fishres.2016.02.026.
- 524 Kai, M., Shiozaki, K., Ohshimo, S, and Yokawa, K. 2015. Growth and spatiotemporal distribution of
525 juvenile shortfin mako, *Isurus oxyrinchus*, in the western and central North Pacific. *Mar. Freshwater*
526 *Res.* **66** (12), 1176–1190. doi: org/10.1071/MF14316.

- 527 Kristensen, K. 2014. TMB: General random effect model builder tool inspired by ADMB [online]. R
528 package version 1.6.2. Available from <https://cran.r-project.org/web/packages/TMB/index.html>
529 [accessed 18 January 2017]
- 530 Kristensen, K., Thygesen, U.H., Andersen, K.H., and Beyer, J.E. 2014. Estimating spatio-temporal
531 dynamics of size-structured populations. *Can. J. Fish Aquat. Sci.* **71** (2): 326–
532 336.doi:10.1139/cjfas-2013-0151.
- 533 Kristensen, K., Nielsen, A., Berg, C.W., Skaug, H., and Bell, B.M., 2016. TMB: Automatic
534 Differentiation and Laplace Approximation. *J. Stat. Softw.* **70** (5): 1–21.doi:10.18637/jss.v070.i05.
- 535 Lee, H.H., Piner, K.R., Methot Jr, R.D., and Maunder, M.N. 2014. Use of likelihood profiling over a
536 global scaling parameter to structure the population dynamics model: an example using blue marlin in
537 the Pacific Ocean. *Fish. Res.* **158**: 138–146.doi:10.1016/j.fishres.2013.12.017.
- 538 Lindgren, F., Rue, H., and Lindström, J. 2011. An explicit link between Gaussian fields and Gaussian
539 Markov random fields: The SPDE approach. *J. R. Stat. Soc. Ser. C Appl. Stat. Methodol.* **73** (4): 423–
540 498.doi: 10.1111/j.1467-9868.2011.00777.x.
- 541 Lo, N.C., Jacobson, L.D., and Squire, J.L. 1992. Indices of Relative Abundance from Fish Spotter Data
542 based on Delta–Lognormal Models. *Can. J. Fish Aquat. Sci.* **49** (12): 2515–2526.doi:
543 10.1139/f92-278.
- 544 Maunder, M.N., and Punt, A.E. 2004. Standardizing catch and effort data: a review of recent approaches.
545 *Fish. Res.* **70** (2–3), 141–159.doi:10.1016/j.fishres.2004.08.002.
- 546 Mucientes, G., Queiroz, N., Sousa, L., Tarroso, P., and Sims, D.W. 2009. Sexual segregation of pelagic
547 sharks and the potential threat from fisheries. *Biol. Lett.* **5** (2): 156–159.doi:10.1098/RSBL.2008.0761.
- 548 Nakano, H., and Nagasawa, K. 1996. Distribution of pelagic elasmobranchs caught by salmon research
549 gillnets in the North Pacific. *Fish. Sci.* **62** (6): 860–865.doi:10.2331/fishsci.62.860.

- 550 Nakano, H., Okazaki, M., and Okamoto, H. 1997. Analysis of catch depth by species for tuna longline
551 fishery based on catch by branch lines. *Bull. Natl. Rese. Inst. Far. Seas Fish.* 34: 43–62.
- 552 Nielsen, J.R., Kristensen, K., Lewy, P., and Bastardie, F. 2014. A Statistical Model for Estimation of Fish
553 Density Including Correlation in Size, Space, Time and between Species from Research Survey Data.
554 PLOS ONE 9(6): e99151. doi:10.1371/journal.pone.0099151.
- 555 Nishida, T., and Chen, D.G. 2004. Incorporating spatial autocorrelation into the general linear model with
556 an application to the yellowfin tuna (*Thunnus albacares*) longline CPUE data. *Fish. Res.* 70 (2–3):
557 265–274. doi:10.1016/j.fishres.2004.08.008.
- 558 Ohshimo, S., Fujinami, Y., Shiozaki, K., Mikihiro, K., Semba, Y., Katsumata, N., Ochi, D., Matsunaga,
559 H., Minami, H., Kiyota, M., and Yokawa, K. 2016. Distribution, body length, and abundance of blue
560 shark and shortfin mako offshore of northeastern Japan, as determined from observed pelagic longline
561 data, 2000–2014. *Fish. Oceanogr.* 25 (3): 259–276. doi:10.1111/fog.12149.
- 562 Petitgas, P. 1998. Biomass-dependent dynamics of fish spatial distributions characterized by geostatistical
563 aggregation curves. *ICES J. Mar. Sci.* 55 (3): 443–453. doi:10.1006/jmsc.1997.0345.
- 564 Petitgas, P., Doray, M., Huret, M., Masse, J., and Woillez, M. 2014. Modelling the variability in fish
565 spatial distributions over time with empirical orthogonal functions: anchovy in the Bay of Biscay. *ICES*
566 *J. Mar. Sci.* 71 (9): 2379–2389. doi:10.1093/icesjms/fsu111.
- 567 Piner, K.R., Lee, H.H., Kimoto, A., Taylor, I.G., Kanaiwa, M., and Sun, C.L. 2013. Population dynamics
568 and status of striped marlin (*Kajikia audax*) in the western and central northern Pacific Ocean. *Mar.*
569 *Freshwater Res.* 64 (2): 108–118. doi:10.1071/MF12302.
- 570 R Development Core Team. 2013. R: a language and environment for statistical computing. R
571 Foundation for Statistical Computing, Vienna, Austria.

- 572 Roa-Ureta, R., and E. Niklitschek. 2007. Biomass estimation from surveys with likelihood based
573 geostatistics. *ICES J. Mar. Sci.* **64** (9): 1723–1734. doi:10.1093/icesjms/fsm149.
- 574 Semba, Y., Nakano, H., and Aoki, I. 2009. Age and growth analysis of the shortfin mako, *Isurus*
575 *oxyrinchus*, in the western and central North Pacific Ocean. *Environ. Biol. Fish.* **84** (4): 377–391.
576 doi:10.1007/S10641-009-9447-X.
- 577 Semba, Y., Aoki, I., and Yokawa, K. 2011. Size at maturity and reproductive traits of shortfin mako,
578 *Isurus oxyrinchus*, in the western and central North Pacific. *Mar. Freshwater Res.* **62** (1): 20–29.
579 doi:10.1071/MF10123.
- 580 Shelton, A.O., Thorson, J.T., Ward, E.J., and Feist, B.E. 2014. Spatial semiparametric models improve
581 estimates of species abundance and distribution. *Can. J. Fish Aquat. Sci.* **71** (11): 1655–1666. doi.
582 10.1139/cjfas-2013-0508.
- 583 Suzuki, Z., Warashina, Y., and Kishida, M. 1977. The comparison of catches by regular and deep tuna
584 longline gears in the western and central equatorial Pacific. *Bull. Natl. Rese. Inst. Far. Seas Fish.* **15**,
585 51–89.
- 586 Thorson, J.T., and Taylor, I.G. 2014. A comparison of parametric, semi-parametric, and non-parametric
587 approaches to selectivity in age-structured assessment models. *Fish. Res.* **158**: 74–83.
- 588 Thorson, J.T., Ianelli, J.N., Munch, S.B., Ono, K., and Spencer, P.D. 2015a. Spatial delay-difference
589 models for estimating spatiotemporal variation in juvenile production and population abundance. *Can.*
590 *J. Fish. Aquat. Sci.* **72** (12): 1897–1915. doi:10.1139/cjfas-2014-0543.
- 591 Thorson, J.T., Shelton, A.O., Ward, E.J., and Skaug, H. 2015b. Geostatistical delta-generalized linear
592 mixed models improve precision for estimated abundance indices for West Coast groundfishes. *ICES*
593 *J. Mar. Sci.* **72** (9): 1297–1310. doi 10.1093/icesjms/fsu243.

- 594 Thorson, J.T., Skaug, H., Kristensen, K., Shelton, A.O., Ward, E.J., Harms, J., and Benante, J. 2015c. The
595 importance of spatial models for estimating the strength of density dependence. *Ecology*. **96** (5): 1202–
596 1212.doi:10.1890/14-0739.1.
- 597 Thorson, J. T., Fonner, R., Haltuch, M., Ono, K., and Winker, H. 2016. Accounting for spatiotemporal
598 variation and fisher targeting when estimating abundance from multispecies fishery data. *Can. J. Fish.*
599 *Aquat. Sci.* **73**: 1–14. doi:10.1139/cjfas-2015-0598.
- 600 Thorson, J.T., and Kristensen, K. 2016. Implementing a generic method for bias correction in statistical
601 models using random effects, with spatial and population dynamics examples. *Fish. Res.* **175**: 66–74.
602 doi:10.1016/j.fishres.2015.11.016.
- 603 Walker, T.I., 1988. Can shark resources be harvested sustainably? A question revisited with a review of
604 shark fisheries. *Mar. Freshwater Res.* **49** (7): 553–572.doi:10.1071/MF98017.
- 605 Walters, C. 2003. Folly and fantasy in the analysis of spatial catch rate data. *Can. J. Fish Aquat. Sci.* **60** (12):
606 1433–1436.doi:10.1139/f03-152.
- 607 Walter, J.F., J.M. Hoenig, and M.C. Christman. 2014. Reducing bias and filling in spatial gaps in
608 fishery-dependent catch-per-unit-effort data by geostatistical prediction, I. Methodology and
609 simulation. *N. Am. J. Fish. Manage.* **34** (6): 1095–1107.doi:10.1080/02755947.2014.932865.
- 610 Ward, P., and Myers, R.A. 2005. Shifts in open-ocean fish communities coinciding with the commencement
611 of commercial fishing. *Ecology*. **86** (4): 835–847.doi:10.1890/03-0746.
- 612 Wilberg, M.J., Thorson, J.T., Linton, B.C., Berkson, J. 2010. Incorporating time-varying catchability into
613 population dynamic stock assessment models. *Rev. Fish. Sci.* **18** (1): 7–24.
- 614 Zuur, A.E., Ieno, E.N., Walker, N.J., Saveliev, A.A., and Smith, G. M. 2009. Zero-truncated and
615 zero-inflated models for count data. *In* *Mixed effects models and extensions in ecology with R*. Springer
616 Science + Business Media, LLC, New York, pp. 261–293.

617

618 **Tables**

619 Table 1. Summary of the model selection information from A) four analyses, including error distribution of
 620 positive catch model (lognormal or gamma), random field (anisotropic or isotropic), the number of
 621 parameters, the negative log-likelihood (NLL), the reduction in AIC (Δ AIC) from the best-fitting model,
 622 absolute value of the maximum gradient, marginal standard deviation for spatial variation and
 623 apatio-temporal and length variation; and B) eight analyses. , including the catch rate predictor of random
 624 effect. “Null” denotes no random effects, “Station” denotes random effects of statistical station (latitude and
 625 longitude), “Length” denotes random effects of body length, and “Station:Length:Year” denotes random
 626 effects of station, length and year.

627 A)

Model	Error distribution of positive catch model	Random field	Number of parameters	Deviance	Δ AIC	Maximum gradient	Marginal SD of spatial variation	Marginal SD of spatio-temporal and length variation
Model A	Lognormal	Isotropic	30	88261		53	0.065	0.243
Model B	Lognormal	Anisotropic	32	88205		0	0.017	0.198
Model C	Gamma	Isotropic	30	89434	1226		0.005	0.240
Model D	Gamma	Anisotropic	32	89383	1179		0.038	0.207

628

629 B)

Model	Catch rate predictors of random effect (RE)	Number of parameters	Deviance	Percent deviance (%)	Δ AIC	Maximum gradient	Marginal SD of spatial variation	Marginal SD of spatio-temporal and length variation
Model 1	Null	23	99919			11697	0.018	
Model 2	Station	27	98741	1.179		10527	0.019	0.59
Model 3	Length	26	95099	3.689		6883	0.016	
Model 4	Station + Length	30	93718	1.453		5510	0.032	0.61
Model 5	Station: Length: Year	29	88504	5.564		293	0.067	1.84
Model 6	Station + Station: Length: Year	30	88502	0.001		294	0.007	0.29
Model 7	Length + Station: Length: Year						0.145	
Model 8	Station + Length + Station: Length: Year	32	88205	0.337		0	0.017	0.20

630

631 **Figure Legends**

632

633 Fig. 1 Map of the operational areas of Japanese commercial fisheries (mean number of hooks) and
634 sampling areas of length data (length composition) in the western and central North Pacific. The map is
635 drawn using the shallow-set fleet subset used for the analysis.

636

637 Fig. 2 Yearly changes in predicted CPUE relative its average for shortfin mako for (a) four models with
638 two different error distributions with and without anisotropy, and (b) seven models with the explanatory
639 variables sequentially added to the null model. Please see an appendix D for the calculation method of the
640 quantity.

641

642 Fig. 3 Overall spatial distribution of predicted CPUE relative its average for shortfin mako (upper figure)
643 We also plot the nominal CPUE relative to its average (lower figure). Please see an appendix D for the
644 calculation method of the quantity.

645

646 Fig. 4 Yearly changes in predicted CPUE relative its average for shortfin mako (black solid line with
647 filled circle). Grey solid line denotes the nominal CPUE relative to its average, shadow denotes the 95 %
648 confidence intervals, and the horizontal dotted line denotes mean value of relative values (1.0). Please see
649 an appendix D for the calculation method of the quantity.

650

651 Fig. 5 Length (Pre-caudal length) specific changes in predicted CPUE relative to its average for shortfin
652 mako (black solid line with filled circle). Grey solid line denotes the nominal CPUE relative to its average,

653 shadow denotes the 95 % confidence intervals, and the horizontal dotted line denotes mean value of
654 relative values (1.0). Please see an appendix D for the calculation method of the quantity.

655

656 Fig. 6 Overall spatial distribution of predicted CPUE relative its average for three growth stages of
657 shortfin mako:(a) Juvenile :(b) Immature :(c) Subadult and adult. We also plot the nominal CPUE relative
658 to its average for the three growth stages of shortfin mako (right figures). Please see an appendix D for the
659 calculation method of the quantity.

660

661 Fig. 7 Yearly changes in predicted CPUE relative its average (black solid line with filled circle) for three
662 growth stages of shortfin mako :(a) Juvenile :(b) Immature :(c) Subadult and adult. Grey solid line
663 denotes the nominal CPUE relative to its average for the three growth stages of shortfin mako, shadow
664 denotes the 95 % confidence intervals, and the horizontal dotted line denotes mean value of relative
665 values (1.0). We also plot the number of hooks (x 1000), representing the yearly changes of available data
666 for shortfin mako (figure d). Please see an appendix D for the calculation method of the quantity.

667

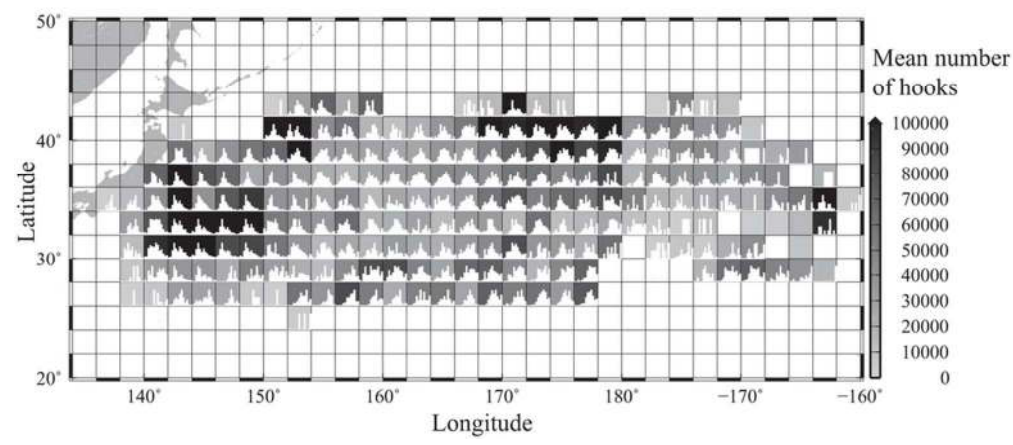
668 Fig. 8. Time (year) specific changes of the spatial distributions of log-scaled predicted CPUE for three
669 growth stages and all combined stages of shortfin mako :(a) Juvenile :(b) Immature :(c) Subadult and
670 adult :(d) All stages. Please see an appendix D for the calculation method of the quantity.

671

672 Fig. 9 Length (Pre-caudal length) and time (year) specific changes in predicted CPUE relative its average
673 for shortfin mako. Black solid line denotes the average length specific distribution across all years,

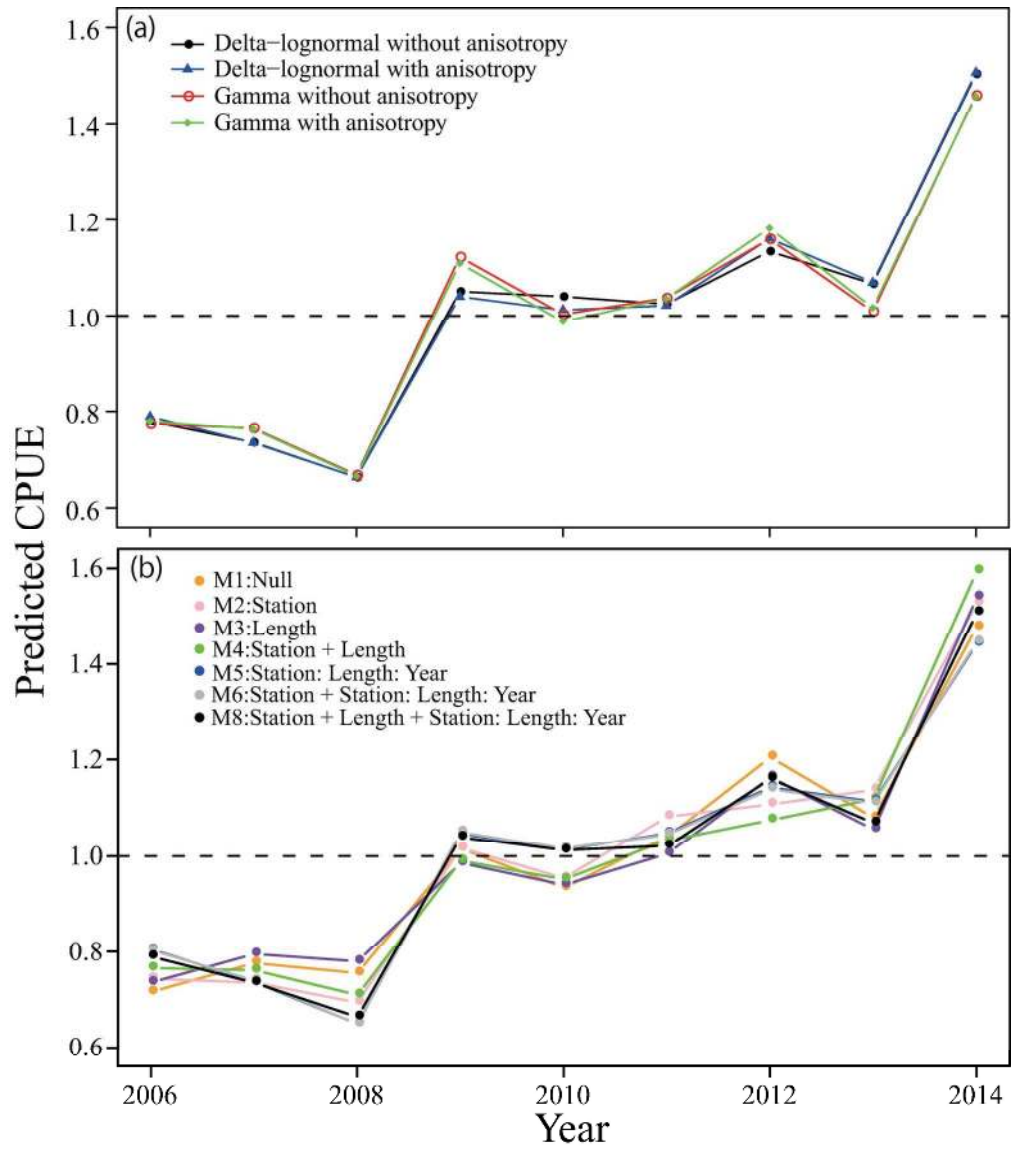
674 shadow denotes the 95 % confidence intervals, and the horizontal dotted line denotes mean value of
675 relative values (1.0). Please see an appendix D for the calculation method of the quantity.

Draft

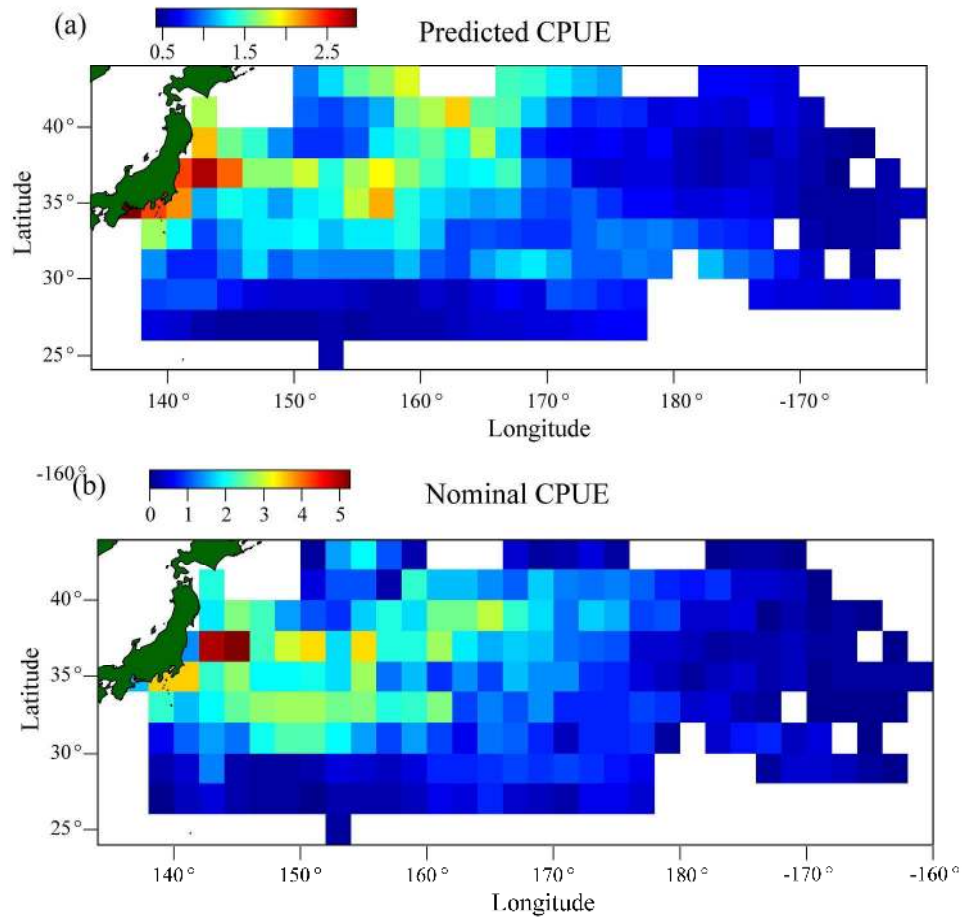


91x40mm (300 x 300 DPI)

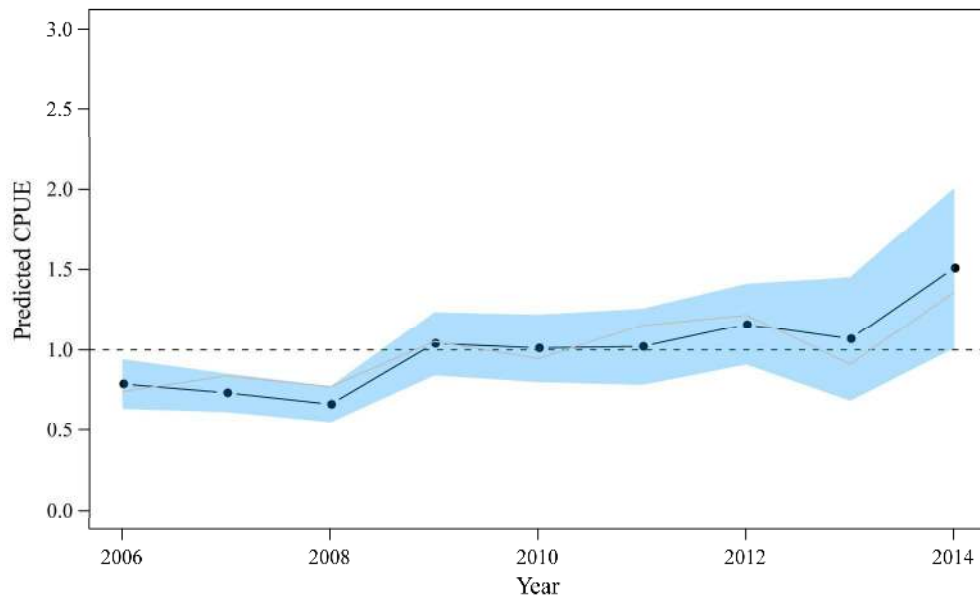
Draft



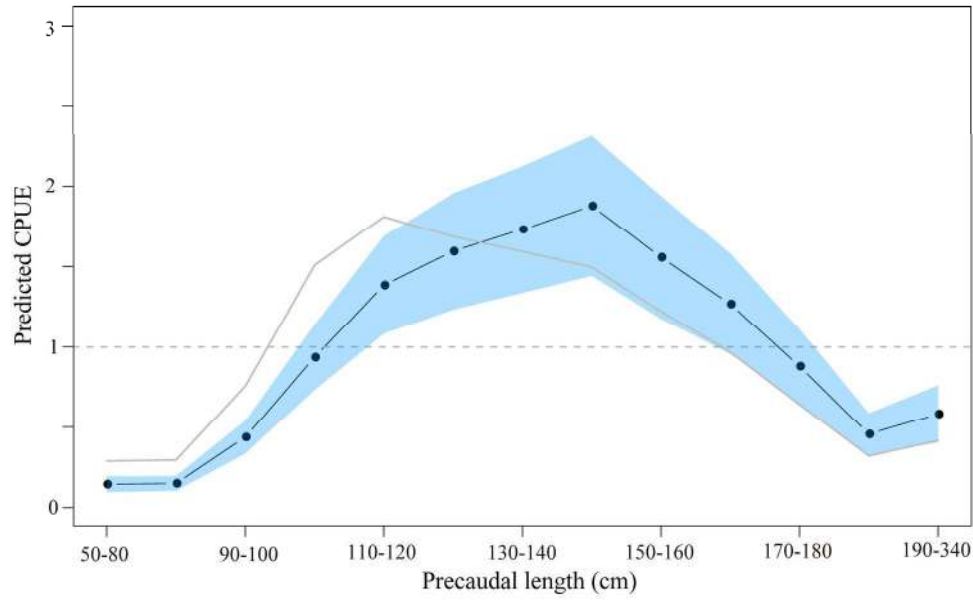
175x201mm (300 x 300 DPI)



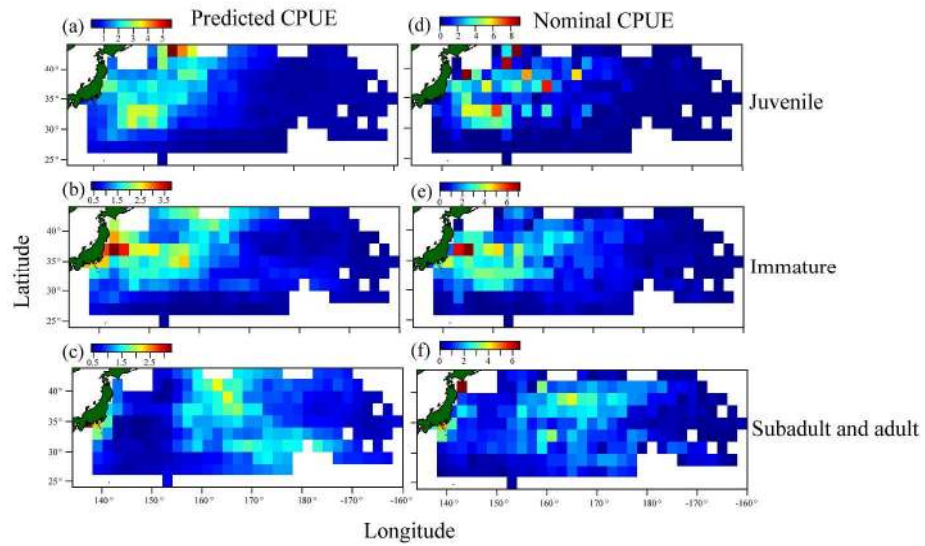
304x365mm (300 x 300 DPI)



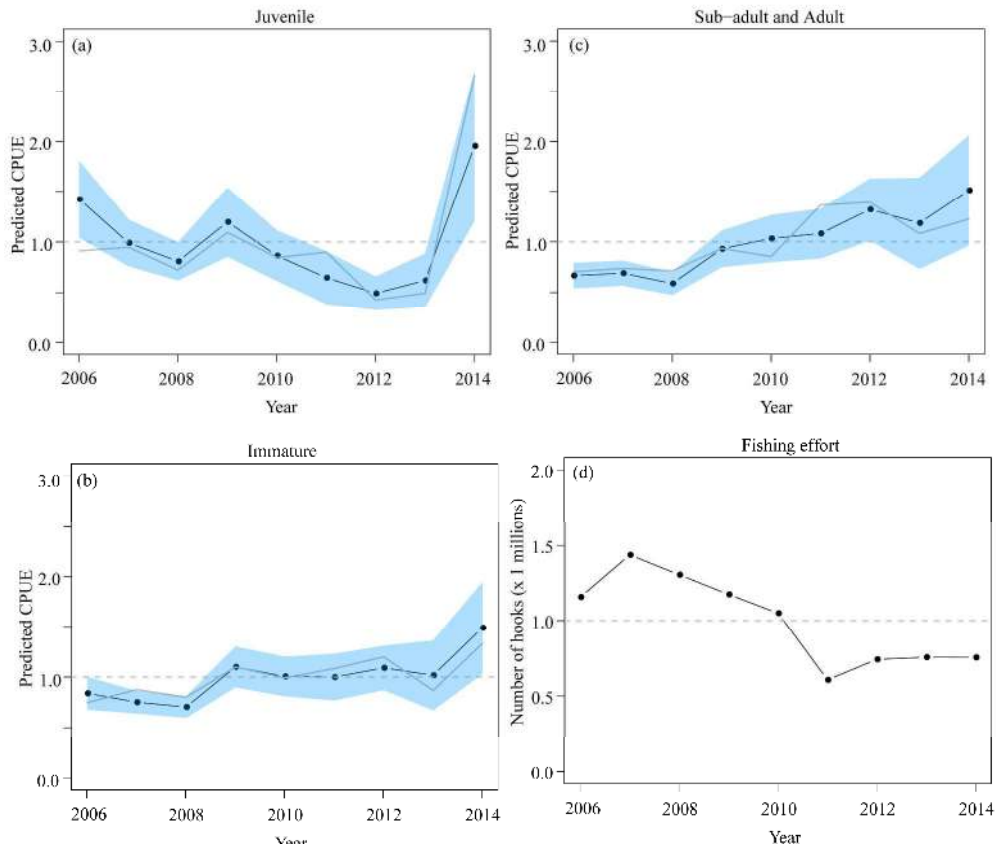
203x135mm (300 x 300 DPI)



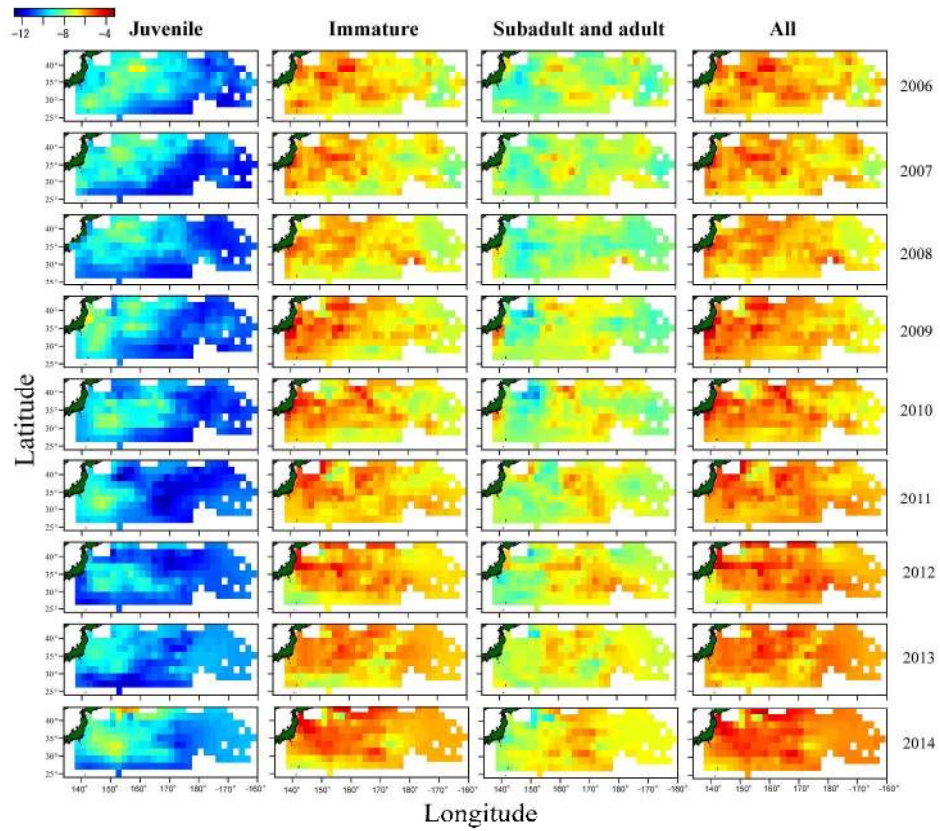
203x135mm (300 x 300 DPI)



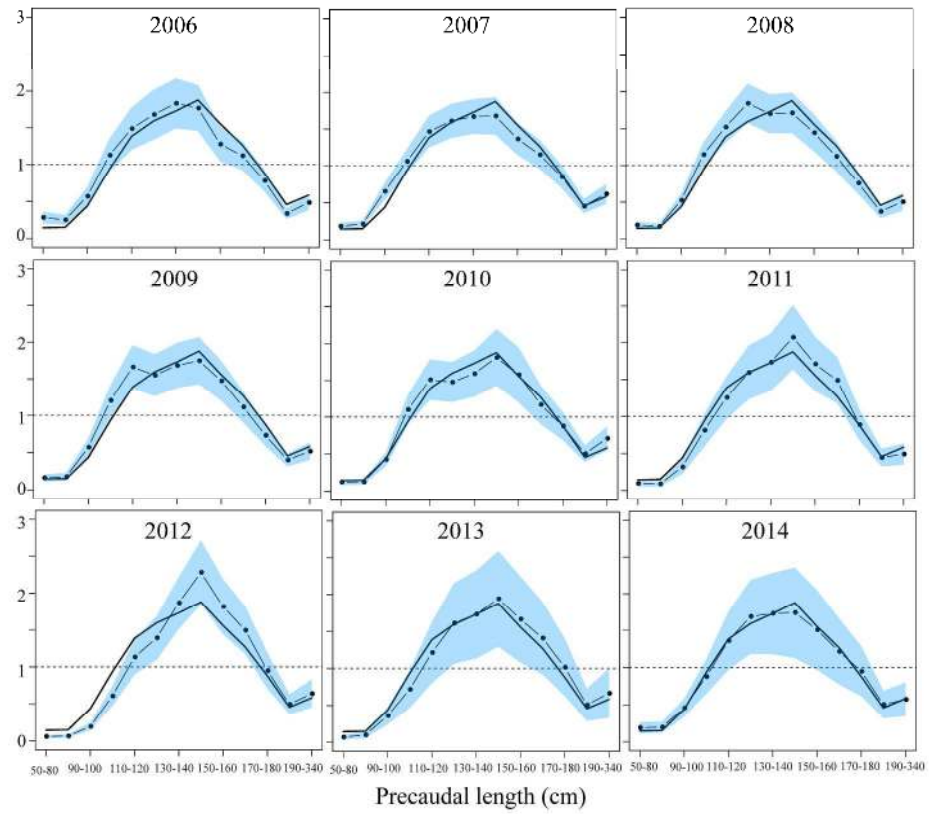
304x304mm (300 x 300 DPI)



304x261mm (300 x 300 DPI)



355x414mm (300 x 300 DPI)



304x261mm (300 x 300 DPI)

1 **Appendices**

2 Appendix A

3 A1. Basic statistical information about shortfin mako catch

4 The proportion of the catch number of mako shark caught by Japanese offshore and distant
5 water shallow-set longliner accounts for approximately 93% (111,318 in number /119,645) to total catch
6 by Japanese offshore and distant water longliner during 2006 and 2014 (if we defined the shallow-set
7 fishery has a gear 3-5 hooks per floats in an operation). Of there, the proportion of the catch number of
8 mako shark caught by Kessenuma boat accounts for approximately 94% (104,864/111,318) to total
9 shallow-set catch during 2006 and 2014. Total number of size sample collected by Kesenuma boat was
10 72,355 during 2006 and 2014.

11

12 A2. Summary of data aggregation

13 (1) For logbook catch data, we aggregated the set-by-set data (i.e. one operation data including year,
14 quarter, latitude and longitude, number of hooks, catch number of shortfin mako and other species) by
15 station (i.e. latitude and longitude) and year-quarter. Set by set data was summed up with regards to
16 the catch number and number of hooks. There is no reduction in the total number of catch as well as
17 hooks in this aggregation.

18 (2) For size data, we aggregated the set-by-set data (i.e. one operation data including year, quarter,
19 latitude and longitude, body length of shortfin mako) by station, year-quarter and length bins. Set by
20 set data was summed up with regards to the total number of catch at each length-interval. There is no
21 reduction in the total number of size data.

22 (3) We combined the catch data with size data based on the same station and same year-quarter. If there
 23 is either (1) no size data at the specific station and in a specific year-quarter, or (2) no catch data at the
 24 specific station and in a specific year-quarter, then we do not include any data for that station and
 25 year-quarter. We summarized the information about the data aggregation in Table A1 and the maps of
 26 nominal CPUE before and after the data aggregation (Fig. A1). Note that the number of set by set data
 27 after aggregation denotes the number of data aggregated by station and year-quarter.

28

29 Appendix B

30 B1. Estimation methods of the random effects (Kristensen et.al. 2016)

31 Let $f(u, \omega)$ denote the negative joint log-likelihood of the data and the random effects. This
 32 depends on the unknown random effects $u \in R^n$ and parameters $\omega \in R^m$, where R is a real n - and m -
 33 space. The TMB package implements maximum likelihood estimation and uncertainty calculations for u
 34 and ω . The maximum likelihood estimate for ω maximizes

$$35 \quad L(\omega) = \int_{R^n} \exp(-f(u, \omega)) du \quad (\text{A1})$$

36 w.r.t. ω . Note that the random effects u have been integrated out and the marginal likelihood $L(\omega)$ is the
 37 likelihood of the data as a function of just the parameters. We use $\hat{u}(\omega)$ to denote the minimizer of $f(u,$
 38 $\omega)$ with respect to u ; i.e.,

$$39 \quad \hat{u}(\omega) = \arg \min_u f(u, \omega) \quad (\text{A2})$$

40 We use $H(\omega)$ to denote the Hessian of $f(u, \omega)$ with respect to u and evaluated at $\hat{u}(\omega)$; i.e.,

$$41 \quad H_{i,j}(\omega) = \frac{\partial^2}{\partial \hat{u}_i(\omega) \partial \hat{u}_j(\omega)} f(\hat{u}(\omega), \omega) \quad (\text{A3})$$

42 The Laplace approximation for the marginal likelihood $L(\omega)$ is

$$43 \quad L^*(\omega) = \sqrt{2\pi^n} \det(H(\omega))^{-0.5} \exp(-f(\hat{u}(\omega), \omega)) \quad (\text{A4})$$

44 We then use a gradient-based nonlinear minimizer to identify the values $\hat{\omega}$ of parameters ω that
45 maximizes this approximation to the marginal likelihood:

$$46 \quad \hat{\omega} = \arg \max_{\omega} L^*(\omega) \quad (A5)$$

47 This approximation is widely applicable including models ranging from non-linear mixed effects models
48 to complex space-time models.

49

50 Appendix C

51 C1. Diagnostics plots of goodness-of-fits

52 The goodness of fits were examined using four types of residual plots obtained from positive
53 catch data: (1) standardized residuals versus the fitted values can assess whether model misspecification is
54 occurring: (2) square root of the absolute values of the standardized residuals versus the fitted values can
55 assess whether the variance changes as a function of the predicted value: (3) the observed versus the
56 predicted values can assess qualitatively whether the explanatory variables are indeed able to reduce the
57 variance in the data: (4) quantile and quantile plots can assess the normality. Overall, the model fit to the
58 data was not bad (Fig. A2). The residuals were slightly biased toward the negative directions.
59 $\text{Sqrt}(\text{Abs}(\text{Residuals}))$ had a tendency to increase as the predicted value was increased. The predicted
60 CPUEs were smaller than observed CPUEs. Q-Q plots indicated that the left ends of the plots were
61 largely deviated from the straight line.

62 We used only the positive catch data to plot the diagnostics because the binomial data with a
63 logistic regression is very complicated to treat the residual patterns. If the true value is 0, we always
64 overestimate the fitted value and residual should be negative. If the true value is 1, we always

65 underestimate the fitted value and residual should be positive. Then, we have two lines of the residual
 66 plots across positive and negative lines.

67

68 Appendix D

69 Calculation method of each quantity

70 Annual abundance (i.e. CPUE which is defined as catch number over number of hooks) is
 71 calculated as the sum of abundance for each station and length interval, averaged across quarter:

$$72 \quad d(t) = \sum_{s=1}^{226} \sum_{l=1}^{13} d(s, t, q, l), \quad (\text{A6})$$

73 where $d(s, t, q, l)$ is defined in Eq. (1), $d(t)$ is total abundance at year t . The overall year relative to its
 74 average is

$$75 \quad d^*(t) = d(t) / \left(\frac{1}{n_t} \sum d(t) \right). \quad (\text{A7})$$

76 Nominal CPUE for combined stations, length interval and quarter is calculated as follows:

$$77 \quad u(t) = \sum_{s=1}^{226} \sum_{q=1}^4 \sum_{l=1}^{13} c(s, t, q, l) / \sum_{s=1}^{226} \sum_{q=1}^4 \sum_{l=1}^{13} f(s, t, q, l) \quad (\text{A8})$$

78 where $u(t)$ is nominal cpue at year t defined by a division of catch number c averaged over s , q , and l
 79 divided by number of hooks f averaged over s , q , and l . The overall year relative to its average is

$$80 \quad u^*(t) = u(t) / \left(\frac{1}{n_t} \sum u(t) \right). \quad (\text{A9})$$

81 The coefficient of variation (CV) for estimated CPUE for combined three growth stages in year t is
 82 calculated as:

$$83 \quad CV(d(t)) = \frac{SE(d(t))}{d(t)} \quad (\text{A10})$$

84 where $CV(d(t))$ is the coefficient of variation of total abundance in year t and $SE(d(t))$ is the
 85 standard error for annual abundance (as estimated using Template Model Builder).

86 Length specific changes in abundance are calculated as the sum of abundance for each station
 87 and year, averaged across quarter:

$$88 \quad d(l) = \sum_{s=1}^{226} \sum_{t=1}^9 d(s, t, q, l), \quad (\text{A11})$$

89 where $d(s, t, q, l)$ is defined in Eq. (1), $d(l)$ is total abundance at length-bin l . The overall length intervals
 90 relative to its average is

$$91 \quad d^*(l) = d(l) / \left(\frac{1}{n_l} \sum d(l) \right). \quad (\text{A12})$$

92 Nominal CPUE for combined stations, overall year and quarter is calculated as follows:

$$93 \quad u(l) = \sum_{s=1}^{226} \sum_{q=1}^4 \sum_{t=1}^9 c(s, t, q, l) / \sum_{s=1}^{226} \sum_{q=1}^4 \sum_{t=1}^9 f(s, t, q, l) \quad (\text{A13})$$

94 where $u(l)$ is nominal cpue at length interval l defined by a division of catch number c averaged over $s, q,$
 95 and t divided by number of hooks f averaged over $s, q,$ and t . The overall length interval relative to its
 96 average is

$$97 \quad u^*(l) = u(l) / \left(\frac{1}{n_l} \sum u(l) \right). \quad (\text{A14})$$

98 The coefficient of variation (CV) for estimated CPUE at length interval l is calculated as:

$$99 \quad CV(d(l)) = \frac{SE(d(l))}{d(l)} \quad (\text{A15})$$

100 where $CV(d(l))$ is the coefficient of variation of total abundance at length-interval l and $SE(d(l))$ is
 101 the standard error for annual abundance (as estimated using Template Model Builder).

102 In the following, we presented and interpreted maps of density that include the effect of fixed
 103 effects and random effects. Here, the average spatial distribution of predicted catch rate for each year was
 104 calculated as:

$$105 \quad \bar{d}(s, t) = \sum_{l=1}^{13} d(s, t, q, l) \quad (\text{A16})$$

106 where $d(s, t, q, l)$ is defined in Eq. (1), $\bar{d}(s, t)$ is the density at location s and time t summed over
107 length intervals l is 13, the sum of quarter q is omitted because q is a fixed effect with no interactions, and
108 where plot the density:

$$109 \quad d_t^*(s) = \frac{d(s,t)}{\left(\frac{1}{n_s} \sum d(s,t)\right)} \quad (A17)$$

110

111 Appendix E

112 The influence of the target changes

113 Swordfish catch ratios (i.e., CPUE) were ranked based on ten equal percentile categories (e.g., 0
114 to <10 %, 10 to <20 %, etc.) for each year, and the ranks were used as target indicators (Hiraoka et al.
115 2016). We used the catch number records for swordfish and blue shark from the same set-by-set logbook
116 data as used for the prediction of the CPUE for shortfin mako. We evaluated the influence of the target
117 changes through a comparison with the annual trends in the CPUE using the best-fitting model with and
118 without target indicator. For example, a set with the highest swordfish CPUE within certain years would
119 be categorized as rank 10, indicating that blue shark was relatively under-targeted in that set.

120

121 Appendix references

122 Hiraoka, Y., Kanaiwa, M., Ohshimo, S., Takahashi, N., Kai, M., and Yokawa, K. 2016. Trend in the
123 relative abundance of the blue shark *Prionace glauca* based on the activities of Japanese distant water
124 and offshore longliners in the North Pacific. *Fish. Sci.* **82**: 687-699.
125 Kristensen, K. 2014. TMB: General random effect model builder tool inspired by ADMB [online]. R
126 package version 1.6.2. Available from <https://cran.r-project.org/web/packages/TMB/index.html>
127 [accessed 18 January 2017]

128

129 **Appendix tables**

130 Table A1 Summary of data aggregation by A) year and B) quarter.

131 A)

Year	Catch number of mako shark (before)	Catch number of mako shark (after)	Number of size data (before)	Number of size data (after)	Number of set by data (before)	Number of set by data (after)	Positive catch ratio of set by set data (before)	Positive catch ratio of set by set data (after)	Number of hooks (before)	Number of hooks (after)
2006	13,180	10,299	7,800	7648	5123	3200	0.57	0.53	18,583,512	15,319,327
2007	15,139	14,460	13,130	12702	5823	4022	0.58	0.50	21,148,480	18,876,303
2008	12,532	12,080	10,571	10113	5312	3610	0.61	0.52	19,185,566	17,139,978
2009	15,751	14,802	8,008	7936	4582	3290	0.65	0.49	16,220,017	15,345,066
2010	13,202	11,907	6,282	6238	4181	2702	0.64	0.48	15,388,103	13,785,927
2011	9,208	8,398	4,777	4705	2356	2145	0.73	0.44	8,766,168	7,958,559
2012	11,202	10,833	6,918	6841	2900	2473	0.66	0.51	10,506,429	9,710,781
2013	8,547	8,257	5,420	5310	3192	2363	0.65	0.48	10,866,447	9,909,735
2014	12,557	12,292	9,449	9389	3072	2231	0.75	0.57	10,216,910	9,838,298

132

133 B)

Quarter	Catch number of mako shark (before)	Catch number of mako shark (after)	Number of size data (before)	Number of size data (after)	Number of set by data (before)	Number of set by data (after)	Positive catch ratio of set by set data (before)	Positive catch ratio of set by set data (after)	Number of hooks (before)	Number of hooks (after)
1	33,729	32,561	21,908	21,605	10,785	5,633	0.69	0.54	37,990,354	36,575,575
2	30,343	26,183	16,598	16,084	9,191	8,753	0.64	0.44	33049087	29,311,644
3	20,075	19,053	14,399	14,158	6,222	5,442	0.69	0.49	22511714	20,889,069
4	27,171	25,531	19,450	19,035	10,343	6,208	0.53	0.56	37330477	31,107,685

134

135

136

137 Table A2. List of all parameters and the estimates for the best-fitting model.

No	Parameter name	Symbol	Type	Estimates
1	Distance of correlation (Spatial random effect)	κ	Fixed	0.27
2	Northings anisotropy	h_1	Fixed	1.46
3	Anisotropic correlation	h_2	Fixed	0.98
4	Parameter governing pointwise variance (Spatial random effect)	η_ν	Fixed	1.43
5	Parameter governing pointwise variance (Length random effect)	η_τ	Fixed	0.30
6	Parameter governing pointwise variance (Spatio-temporal and length random effect)	η_θ	Fixed	0.23
7	Correlation parameter of length bins	ψ	Fixed	0.17
8	Parameter governing autocorrelation (Length random effect)	ρ_τ	Fixed	0.16
9	Parameter governing autocorrelation (spatio-temporal and length random effect)	ρ_θ	Fixed	0.85
10-18	Intercept for year	d_0	Fixed	Not shown
19-21	Temporal variance (quarter effect) ^a	δ	Fixed	Not shown
22	Scale parameter of zero catch ratio	z_1	Fixed	0.74
23	Scale parameter of zero catch ratio	z_0	Fixed	2.73
24-32	Log-standard deviation for catch rates for year	σ	Fixed	Not shown
33	Spatial residuals	γ	Random	Not shown
34	Length residuals	τ	Random	Not shown
35	Spatio-temporal and length residuals	θ	Random	Not shown

138

139 a: Offset of density in quarter 2-4 from density in quarter 1

140

141 Table A3. Summary of yearly changes in CPUE predicted by spatio-temporal model for three (“Juvenile”, ”Immature”, and ”Subadult and adult”)

142 and a combined (“All”) growth stages along with the corresponding estimates of the coefficient of variation (CVs), and yearly changes in the nominal

143 CPUE and fishing effort (number of hooks x 1millions). The values are predicted using the best fitting model and scaled by average CPUE.

Year	Predicted				Nominal				CV				Effort
	All	Juvenile	Immature	Adult	All	Juvenile	Immature	Adult	All	Juvenile	Immature	Adult	All
2006	0.79	1.42	0.84	0.67	0.74	0.91	0.75	0.70	0.10	0.14	0.10	0.10	0.10
2007	0.73	0.99	0.75	0.69	0.84	0.95	0.88	0.74	0.08	0.12	0.08	0.09	0.08
2008	0.66	0.81	0.70	0.59	0.77	0.72	0.80	0.71	0.08	0.12	0.08	0.10	0.08
2009	1.04	1.20	1.10	0.93	1.05	1.09	1.10	0.93	0.09	0.15	0.09	0.10	0.10
2010	1.01	0.86	1.01	1.03	0.95	0.85	0.99	0.85	0.10	0.15	0.10	0.12	0.11
2011	1.02	0.65	1.00	1.08	1.16	0.90	1.08	1.36	0.12	0.21	0.12	0.12	0.12
2012	1.16	0.49	1.09	1.32	1.22	0.43	1.20	1.39	0.11	0.17	0.10	0.12	0.11
2013	1.07	0.62	1.02	1.18	0.91	0.49	0.87	1.08	0.18	0.22	0.17	0.19	0.18
2014	1.51	1.96	1.49	1.51	1.36	2.66	1.33	1.22	0.17	0.20	0.16	0.19	0.17

144

145

146 **Appendix Figure Legends**

147

148 Fig. A1 Maps of log-scaled nominal CPUE (catch/number of hooks x1000) by station before and
149 after the data aggregation.

150

151 Fig. A2 Diagnostic plots of goodness-of-fit for the most parsimonious model selected by AIC.

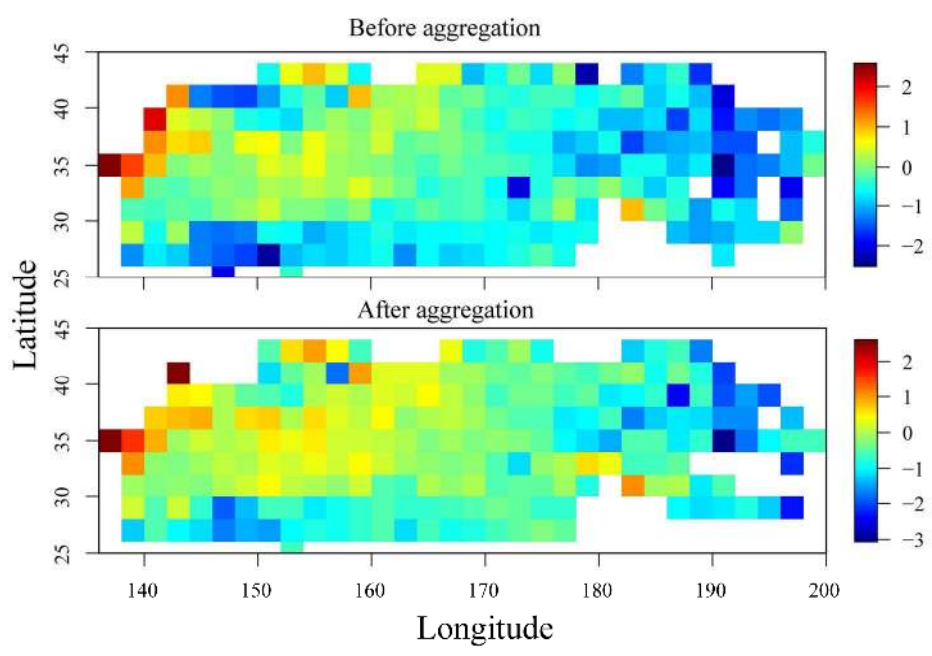
152

153 Fig. A3 Yearly changes in predicted CPUE relative its average for shortfin mako (black solid line
154 with filled circle) with target effect (solid line with filled circle) and without target effect (solid line
155 with filled triangle). Target effect (Hiraoka et al., 2016) is defined as a ranking of swordfish catch
156 ratio (i.e., CPUE for each set) based on ten equal percentile categories (e.g., 0 to <10 %, 10 to <20
157 %, etc.) for each year. Grey solid line denotes the nominal CPUE relative to its average, and the
158 horizontal dotted line denotes mean value of relative values (1.0).

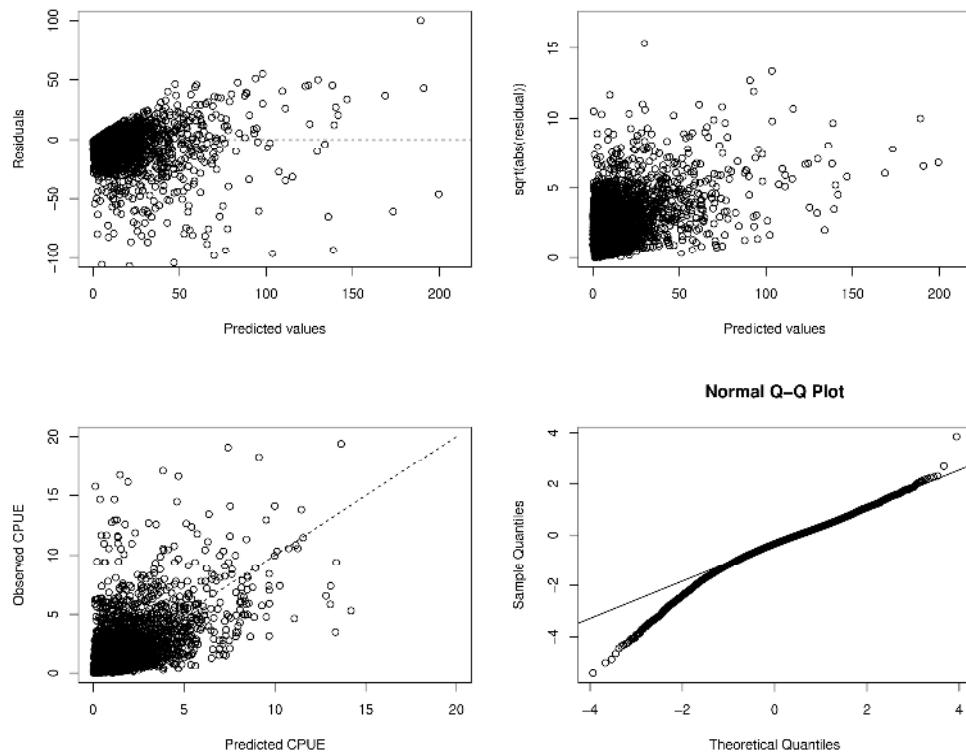
159

160

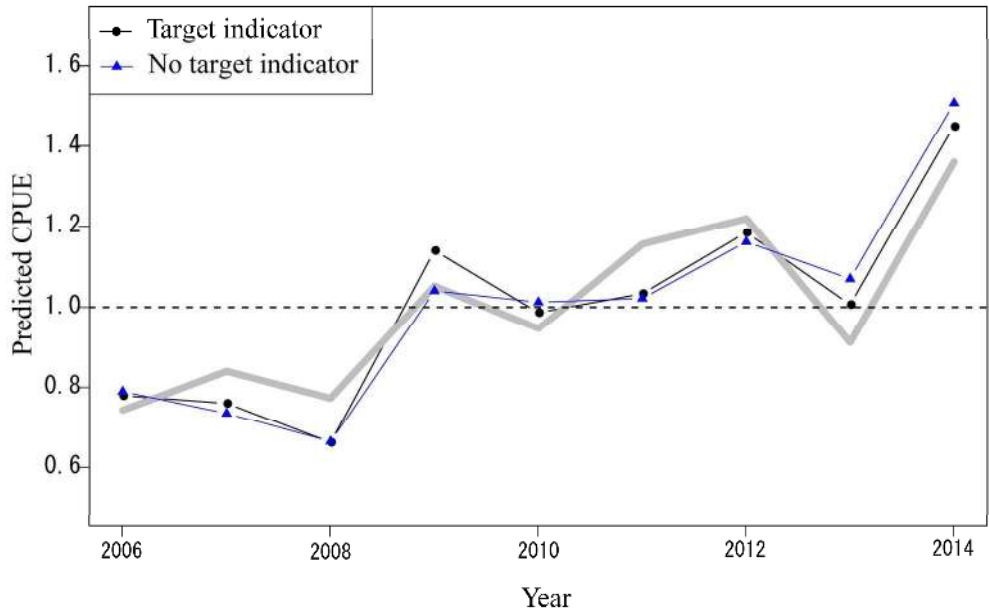
Draft



203x162mm (300 x 300 DPI)



254x211mm (300 x 300 DPI)



203x135mm (300 x 300 DPI)